Diplomarbeit

ON-CHIP PARTICLE SEPARATOR BASED ON DIELECTROPHORESIS

Ausgeführt zum Zwecke der Erlangung des akademischen Grades eines Diplom-Ingenieurs

unter der Leitung von

Univ. Prof. Dr. Michiel J. Vellekoop

und

Dipl.Ing. Jeroen H. Nieuwenhuis

Institut für Sensor- und Aktuatorsysteme

eingereicht an der Technischen Universität Wien

Fakultät für Elektrotechnik und Informationstechnik

von

Stefan KOSTNER

Matr.Nr. 9826179

Ortliebgasse 33/18, 1170 Wien

Wien, im Mai 2004

Abstract

In this project a particle separator chip based on dielectrophoresis was developed. Dielectrophoresis is the effect that polarizable particles experience a force when they are exposed to a non-uniform electric field. The dependency of this phenomenon on the particle size is exploited to separate particles of different size in a microfluidic channel.

In the device a separation of particles is established by forcing them on trajectories of certain mean velocities in a pressure driven flow. In order to manipulate these paricles dielectrophoretic forces are applied.

This work covers the full development cycle beginning with the construction of a model based on electric field and liquid flow simulations, the design and fabrication, and ending with the characterization of the device.

Experimental proof of concept is given by retention time measurements of small particles (8 and 15μm, respectively) with the fabricated device.

Kurzfassung

Im Rahmen dieses Projekts wurde ein Partikel-Separator-Chip auf Grundlage des Effekts der Dielektrophorese entwickelt. Dielektrophorese ist ein Phänomen bei dem sich eine Kraft auf ein polariserbares Teilchen aufbaut wenn selbiges einem nicht homogenen elektrischen Feld ausgesetzt ist. Die Abhängigkeit dieses Effekts vom Partikelradius wird in dem voliegenden Fall ausgenutzt um Partikel, abhängig von ihrer Größe, in einem mikrofluidischen Kanal voneinander zu separieren.

In der durch Druck aufgebauten Strömung wird eine Separation dadurch erreicht, daß die einzelnen Partikel auf Trajektorien geleitet werden, die eine unterschiedliche Durchschnittsgeschwindigkeit aufweisen. Dielektrophoretische Kräfte werden dazu benutzt die Partikel in der Strömung abzulenken.

Die vorliegende Arbeit behandelt den vollständigen Entwicklungszyklus beginnend mit der Konstruktion eines Models basierend auf Simulationen von elektrischem Feld und fluidischem Strömungsfeld, Design und Herstellung sowie der Charakterisierung des Chips.

Die Funktionsweise wurde anhand von Messungen der Durchlaufzeit verschieden kleiner Partikel (8 und 15μm) demonstriert.

Acknowledgments

First and foremost, I would like to thank to Univ. Prof. Dr. Michiel J. Vellekoop for making this project possible. His engagement and advices combined with the provided equipment brought this project to a full success. Special thanks to my adviser Dipl.-Ing. Jeroen H. Nieuwenhuis for his support and the willingness to spend endless hours for constructive conversations and encouragement in relevant situations.

I would like to thank to the people involved in technology which are (in alphabetical order): Dr. Artur Jachimowicz, Dr. Johannes Schalko, Ing. Edeltraud Svasek and Ing. Peter Svasek. Their maximum employment raised my ideas to real live.

Many thanks to Univ. Lektor Günther Stangl who encouraged me to join this institute for doing my thesis and for borrowing equipment.

Furthermore I want to thank to my parents Margret and Alois Kostner for their mental and financial support all the years.

Special thanks to my girlfriend Barbara Neuherz for support and believing in me.

Thanks also to my room mates Franz Klinger, Martin Strobach and Bernhard Valentin for their comments and ideas.

Finally I would like to thank to the State of Austria for the financial support in form of a scholarship.

Nomenclature

$\mathbf{D}$	electric flux density vector
$\mathbf{E}$	electric field vector
F_B	buoyancy force
F_D	drag force
F_{DEP}	dielectrophoretic force
F_G	gravity force
F_I	inertia force
K	Clausius Mossotti Factor
Q	electric charge
R	particle radius
Re	Reynolds Number
V	volume
$\mathbf{e_r}$	radial direction
$\mathbf{p}$	dipole moment
p_{eff}	effective dipole moment
r	radius (variable)
v_l	local liquid velocity
v_p	particle velocity
Φ	electrostatic potential
Θ	azimuthal angle
ε_1	relative permittivity of liquid
ε_2	relative permittivity of particle
η	viscosity of the liquid
ρ, ρ_p, ρ_l	mass density (particle, liquid)

Contents

Chapter 1

Introduction

Microfluidics is a very agile field of research these days. On one hand it seems very attractive to deal with small sample volumes for example in blood analysis. On the other hand the scaling to small devices allows for the utilization of effects which do not appear in the large scale. As a typical example the dielectrophoretic force on a particle can be mentioned as an effect which is only noticeable if a large non-uniformity of an electric field within the particle dimensions is present. Such large non-uniformities can be established when the actuating electrodes are in the size range of the particles and this requests for small measurements of used devices.

Particle separation can be considered as a task necessary for several lab-on-a-chip applications. Furthermore there are other areas of application like cancer research, industrial process monitoring and medical applications.

In this work a particle separator chip based on dielectrophoresis was developed. Here, the term particle separation means a separation of different particles in the time domain while sorting is a term used for the spatial domain. Our device is capable for slowing down particles depending on their size and in such a way that a separation in the time domain is established.

Dielectrophoresis has some advantages which makes it very attractive as an actuation principle for particle research. First, its absolute value (in a first order approximation) is proportional to the third power of the particle diameter. Therefore, a discrimination on the particle size should in principle be very sensitive. Furthermore, the involved particles only have to be polarizable (which is the case for biologic objects like cells) but not charged.

In the first section the theory of forces on particles in liquids including the dielectrophoretic force is addressed. Then a model for the particle behavior is presented which is the basis for the investigation of different electrode designs. An optimization yields to a specific design which was then realized. Measurements as well as a discussion of the results are presented which yields proposals for improvements of the device.

Chapter 2

Theory

2.1 Introduction

One of the goals of this project was to develop a model for the behavior of a particle in a microfluidic device. Therefore it is of importance to understand the nature of the forces which appear if a particle is exposed to the fields given in such a case. With this knowledge it is possible to simulate different scenarios.

In the following sections the theory of forces is developed which deals with particles that are exposed to an electric field and to a liquid flow field. The scenario taken as a basis is outlined in figure 2.1. A polarizable particle with a given radius is located in a liquid which is in motion. Additionally an electric field is applied to this liquid. Both the liquid motion and the electric field affect the particle and cause forces acting on it.

These acting forces are summarized here:

- v_l is the velocity field of the liquid surrounding the particle. The flow profile (constant in fig. 2.1) depends on the channel geometry. If the particle moves with a lower velocity than the liquid flow ($v_p < v_l$) it will be dragged in positive x-direction by the *drag force* F_D (see section 2.3). In the case that $v_p > v_l$ the force F_D has a negative sign.

- The particle is also exposed to an electric field **E** which is in our case non-uniform. In a first assumption, we expect a *dielectrophoretic (DEP) force* F_{DEP} in positive y-direction considering negative dielectrophoresis (see section 2.2).

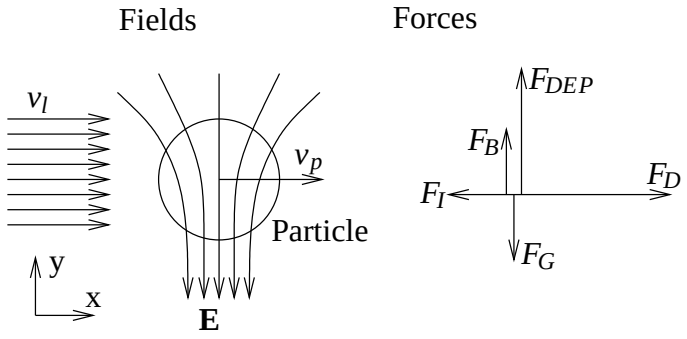

Figure 2.1: Forces acting on a particle

- If the particle and the surrounding liquid have different mass densities, it is of importance to take the *buoyancy force* F_B and the *gravity force* F_G into account (also outlined in Section 2.3). Both can be treated as constant forces depending on the mass densities of particle and liquid. In the case that the mass densities of both materials have the same value these forces are in balance and can therefore be neglected.

- Since the particle is accelerated due to forces described above, there will also be an inertia effect which depends on the mass and on the acceleration of the particle. The sign of this *inertia force* (F_I) is always contrary aligned to the vectorial sum of all acceleration forces. This force is introduced in the continuous model (Section 2.5) and is not separately addressed.

These above listed forces which affect the behavior of the particle are discussed in detail in the following sections. The resulting mathematical expressions are merged together by means of a force equilibrium (see section 3.4). As a result a first order linear differential equation delivers the solutions for specific initial conditions (eq. (2.41)).

2.2 Theory of dielectrophoresis (DEP)

2.2.1 Introduction

Dielectrophoresis is defined as the motion of an uncharged polarizable particle in a non-uniform electric field due to induction [Jon95]. The electric field induces a dipole moment in the particle. If the electric field is non-uniform, a force appears. In the following sections the derivation of this force is presented. Therefore, the *effective dipole moment method* is used, which means that an expression for the so called *effective dipole moment* is found in order to calculate the force in the same way as for common dipoles. This method is taken from [Jon95] and is carried out here in detail in order to be able to estimate the consequences of the assumptions which are used.

2.2.2 Calculation of the dielectrophoretic force $\mathbf{F_{DEP}}$

In this section the dielectrophoretic force on a particle in a suspending medium exposed to an electric field $\mathbf{E}$ is calculated.

First the force on an uncharged dipole like shown in figure 2.2 is investigated by calculating the resulting *Coulomb Force* on both charges q and $-q$:

$$\mathbf{F} = q\mathbf{E}(\mathbf{r}+\mathbf{d}) - q\mathbf{E}(\mathbf{r}). \tag{2.1}$$

A taylor series of $\mathbf{E}$ developed in the point $\mathbf{r}$, truncated after the linear element and calculated in the point $\mathbf{r}+\mathbf{d}$ for $\mathbf{d} << \mathbf{r}$ gives:

$$\mathbf{E}(\mathbf{r}+\mathbf{d}) = \mathbf{E}(\mathbf{r}) + \nabla\mathbf{E}(\mathbf{r})\cdot\mathbf{d} + \ldots \tag{2.2}$$

Insert equation (2.2) in equation (2.1) leads to

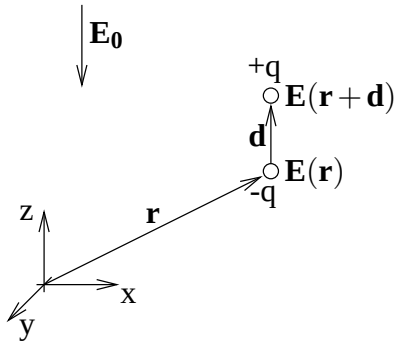

Figure 2.2: Common dipole in an electric field.

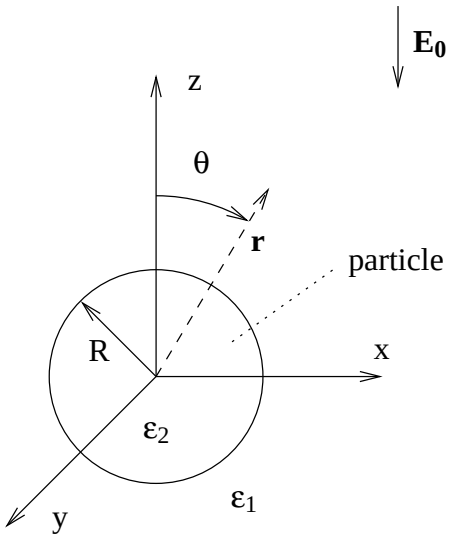

Figure 2.3: Particle in an electric field.

$$\mathbf{F} = \underbrace{q\mathbf{d}}_{\mathbf{p}} \cdot \nabla \mathbf{E} = \mathbf{p} \cdot \nabla \mathbf{E}. \tag{2.3}$$

$\mathbf{p} = q\mathbf{d}$ is defined as the dipole moment. It turns out that a non-uniform electric field ($\nabla\mathbf{E}$) is necessary in order to establish a resulting force on the dipole.

Equation (2.3) gives information about the force acting on a static dipole moment. If a polarizable particle is placed in an electric field an induced dipole moment can be expected. For the calculation of the force on such a particle using equation (2.3) the induced dipole moment has to be determined. This is done by comparing the electrostatic potentials of a common dipole to that of a polarizable sphere exposed to an electric field.

First the potential of a point charge is calculated which is then generalized to that of a point dipole. The electric flux density $\mathbf{D}$ of a sphere with the charge Q at the radius r is:

$$\mathbf{D} = \varepsilon\mathbf{E} = \frac{Q}{4\pi r^2}\mathbf{e_r} \quad \text{where } \varepsilon = \varepsilon_0\varepsilon_r. \tag{2.4}$$

$\mathbf{e}_r$ is the basis vector in radial direction. Then the electric field and the electrostatic potential

$\Phi(r)$ can be determined:

$$\rightarrow \mathbf{E} = \frac{Q}{4\pi\varepsilon r^2}\mathbf{e_r} \tag{2.5}$$

$$\rightarrow \Phi(r) = -\int \mathbf{E}d\mathbf{r} = \frac{1}{4\pi\varepsilon}\frac{Q}{r}. \tag{2.6}$$

The electrostatic potential of a point dipole can be found by superposition of the potentials of two opposite charges using equation (2.6):

$$\Phi = \frac{Q}{4\pi\varepsilon}(\frac{1}{r_1} - \frac{1}{r_2}) \tag{2.7}$$

$$\mathbf{r} = x\mathbf{e_x} + y\mathbf{e_y} + z\mathbf{e_z} \tag{2.8}$$

$$\frac{1}{r_1} = (x_1^2 + y_1^2 + (z_1 - \frac{d}{2})^2)^{-\frac{1}{2}} \tag{2.9}$$

A taylor series for $d \ll r_1$ gives:

$$\frac{1}{r_1} = (x_1^2 + y_1^2 + z_1^2)^{-\frac{1}{2}} - \frac{1}{2}(x_1^2 + y_1^2 + z_1^2)^{-\frac{3}{2}} z_1 \frac{d}{2} + \ldots \approx \frac{1}{r} + \frac{1}{2}\frac{dz}{r^3} \tag{2.10}$$

$$\frac{1}{r_2} = \frac{1}{r} - \frac{1}{2}\frac{dz}{r^3} \tag{2.11}$$

$$\rightarrow \frac{1}{r_1} - \frac{1}{r_2} = \frac{dz}{r^3} = \frac{d}{r^2}cos(\theta) \tag{2.12}$$

Using (2.12) in (2.7) gives:

$$\Phi = \frac{p}{4\pi\varepsilon}\frac{cos(\theta)}{r^2} \tag{2.13}$$

where $p = Qd$ is the absolute value of the dipole moment.

Now an expression for the electrostatic potential of an induced dipole is calculated. If a polarizable particle is exerted to an electric field, a dipole moment is induced. For calculating the force on a particle, the *effective moment* method is introduced. The effective moment p_{eff} is defined as the moment of an equivalent point dipole producing the same electrostatic potential as a common dipole.

The electrostatic potential outside and inside a sphere exposed to an electric field is (fig. 2.3):

$$\Phi_1(r,\theta) = -E_0 r cos(\theta) + A\frac{cos(\theta)}{r^2} \quad \text{for } r > R \tag{2.14}$$

$$\Phi_2(r,\theta) = -Br cos(\theta) \quad \text{for } r < R \tag{2.15}$$

This includes the assumption, that the electrostatic potential consists of a part coming from the external uniform field $\mathbf{E_0}$ and another part coming from the point dipole itself. The two unknown constants A and B can be verified by applying the following boundary conditions to the sphere boundaries:

$$\Phi_1(r = R,\theta) = \Phi_2(r = R,\theta) \tag{2.16}$$

$$\varepsilon_1\frac{\partial\Phi_1(r = R,\theta)}{\partial r} = \varepsilon_2\frac{\partial\Phi_2(r = R,\theta)}{\partial r} \tag{2.17}$$

Equation (2.16) claims the continuity of the electrostatic potential Φ and equation (2.17) is the formulation of the steadiness of the normal projection of the flux density vector. Using equation (2.14) and (2.15) in equation (2.16) and (2.17) yields in the result:

$$A = E_0 R^3 \frac{\varepsilon_2 - \varepsilon_1}{\varepsilon_2 + 2\varepsilon_1} \tag{2.18}$$

$$B = E_0 \frac{3\varepsilon_1}{\varepsilon_2 + 2\varepsilon_1} \tag{2.19}$$

When we now compare equation (2.13) with the second part in equation (2.14) using equation (2.18) a expression for p_{eff} results:

$$p_{eff} = 4\pi\varepsilon_1 A = 4\pi\varepsilon_1 E_0 R^3 \frac{\varepsilon_2 - \varepsilon_1}{\varepsilon_2 + 2\varepsilon_1} \tag{2.20}$$

Using equation (2.20) in the previously calculated expression for the force on a dipole in a nonuniform field (eq. (2.3)) leads to the following expression:

$$F_{dipole} = 4\pi\varepsilon_1 R^3 K \left|\mathbf{E_0}\right| \mathbf{e_p} \cdot \nabla \mathbf{E_0} \tag{2.21}$$

$\mathbf{e_p}$ is the direction of the dipole moment, K is the so called *Clausius Mosotti Factor* ($K = \frac{\varepsilon_2 - \varepsilon_1}{\varepsilon_2 + 2\varepsilon_1}$). Since we know that the polarization of the particle should always have the same direction as the inducing electric field eq.(2.21) simplifies:

$$\mathbf{F_{DEP}} = 4\pi\varepsilon_1 R^3 K \left|\mathbf{E_0}\right| \mathbf{e_p} \cdot \nabla(\left|\mathbf{E_0}\right| \mathbf{e_p}) = \tag{2.22}$$

$$= 4\pi\varepsilon_1 R^3 K \underbrace{E_0 \nabla E_0}_{\frac{1}{2}\nabla E_0^2} \tag{2.23}$$

$$\mathbf{F_{DEP}} = 2\pi\varepsilon_1 R^3 K \nabla E_0^2 \tag{2.24}$$

Equation (2.24) is the common expression for the dielectrophoretic force acting on a particle in a medium exposed to an electric field.

2.3 Drag force on a particle in a liquid flow

For the calculation of the drag force on a particle in a fluid stream the so called Navier Stokes equations are responsible [Whi01]. These very complex differential equations are generally unsolvable, but there exists an approximation (Stokes approximation) for "'creeping flow"' (Reynolds Numbers < 1) as an easy to use solution:

$$F_D = 6\pi\eta R(v_l - v) = k_1(v_l - v_p). \tag{2.25}$$

F_D is the drag force acting on the particle having its origin in the fluid motion, η is the viscosity, R is the particle radius, v_l is the liquid velocity and v is the particle velocity. The proof for this expression is not given here.

The Reynolds Number for a $15\mu m$ particle in water at a velocity of $v_l = 1.6\frac{mm}{s}$ calculates:

$$Re = \frac{\rho v_l}{\mu} = 0.024 \tag{2.26}$$

which is well below unity.

2.4 Buoyancy and gravity force

The resulting force caused by buoyancy and gravity mainly depends on the mass density difference between particle material and surrounding medium. The buoyancy force calculates

$$F_B = \rho_l g V \tag{2.27}$$

where g is the acceleration of gravity and ρ_l and V are the mass density and the volume of the displaced medium[1] respectively.

The combination of buoyancy and gravity ($F_G = \rho_P g V$) to a resulting force, delivers:

$$F_{BG} = gV(\rho_P - \rho_l). \tag{2.28}$$

It is obvious that same mass densities for particle and fluid result in a force balance between buoyancy and gravity.

2.5 Continuous model

2.5.1 Introduction

In the following sections, the behavior of a particle in a fluid flow exposed to an electric field is modeled using the forces derived in sections 2.2 and 2.3. The combination of all forces to an equilibrium results in a linear first order differential equation. For the given problem it is sufficient to develop a two-dimensional model which in fact consists of two independent submodels, each of which describing the dynamic behavior of the particle in one direction[2]. The only difference is an additional term carrying the buoyancy part. The advantage of this approach is that the problem can be formulated as a scalar problem.

2.5.2 Force Equilibrium

All forces on the particle are summarized below:

- *Dielectrophoretic force*:

$$F_{DEP} = 4\pi\varepsilon_1 R^3 K \nabla E_0^2 \tag{2.29}$$

[1] When a rigid body is immersed in a fluid, a certain amount of this fluid is being displaced.

[2] These two directions (x,y) are orthogonal to each other.

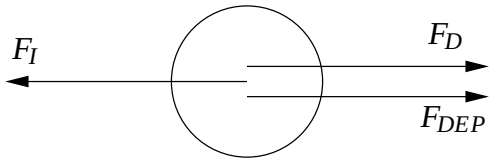

Figure 2.4: Forces for horizontal equilibrium.

- Stokes Approximation for the *drag force*. If the particle is slower than the surrounding medium it is dragged in the direction of the flow (positive sign).

$$F_D = 6\pi\eta R(v_l - v) = k_1(v_l - v) \quad \text{with } k_1 = 6\pi\eta R \tag{2.30}$$

  η is the viscosity of the surrounding fluid [3], r is the radius of the particle v_l is the velocity of the fluid and v is the velocity of the particle. The sign of this force changes in the point $v = v_l$.

- Inertia force:

$$F = ma = m\frac{dv}{dt} \tag{2.31}$$

  $m = \frac{4}{3}\pi\rho R^3$ is the mass of the particle (ρ is the mass density, R is the radius) and a is the acceleration in $[\frac{m}{s^2}]$.

- Buoyancy/gravity force: If there is a significant difference between the densities of the particle and the fluid the buoyancy and the gravity has also to be considered:

$$F_B = gV(\rho_P - \rho_{fl}) \tag{2.32}$$

The sum of these forces is calculated for the horizontal direction:

$$F_D + F_{DEP} = F_I \tag{2.33}$$

using equation (2.30) and (2.31) this equilibrium calculates to:

$$k_1(v_l - v) + F_{DEP} = m\frac{dv}{dt} \tag{2.34}$$

$$\frac{dv}{dt} + \frac{k1}{m}v = \frac{F_{DEP} + k_1 v_l}{m} \tag{2.35}$$

which is a linear differential equation of first order. Multiplying eq. (2.35) by

$$\sigma = e^{\int \frac{k1}{m} dt} = e^{\frac{k1}{m}t} \tag{2.36}$$

gives

$$\underbrace{e^{\frac{k_1}{m}t}\frac{dv}{dt} + \frac{k1}{m}ve^{\frac{k1}{m}t}} = e^{\frac{k1}{m}t}\frac{F_{DEP} + k_1 v_l}{m} \tag{2.37}$$

$$\frac{d}{dt}[ve^{\frac{k_1}{m}t}] = e^{\frac{k_1}{m}t}\frac{F_{DEP} + k_1 v_l}{m}. \tag{2.38}$$

[3] $\eta = 1.002E-3\frac{kg}{ms}$ for water

Integration over time gives:

$$ve^{\frac{k_1}{m}t} = \frac{F_{DEP} + k_1 v_l}{m} \int e^{\frac{k_1}{m}t} dt = \tag{2.39}$$

$$= \frac{F_{DEP} + k_1 v_l}{m} \frac{m}{k_1} e^{\frac{k_1}{m}t} + C \tag{2.40}$$

where C is an integration constant which has to be determined by the initial condition $v(t = 0)$. Then the solution can then be written as follows:

$$v = \frac{F_{DEP} + k_1 v_l}{k_1} + Ce^{-\frac{k_1}{m}t}. \tag{2.41}$$

Equation (2.41) describes the motion of a particle in a fluid flow with the velocity v_l and exposed to a dielectrophoretic force (F_{DEP}) in a horizontal axis. For the vertical solution an additional buoyancy force term has to be considered (eq. (2.32)) which can be seen as an additive value to the DEP force and thereby does not modify the principle structure of the solution ((2.41)).

This model has the following assumptions:

- The expression for the drag force in eq. (2.30) is an approximation for a particle exposed to a flat flow profile. In a pressure driven flow the velocity distribution depends on the shape of the channel and can in most cases not be assumed to be flat (fig. 2.5). For the force calculation the liquid velocity v_l at the center of the particle is used. Additionally a rotation of the particle can be expected due to the velocity gradient.

- The dielectrophoretic force F_{DEP} has been assumed to be constant in equation (2.41). This means that the solution is only valid for a short displacement region. When a trajectory of a particle is calculated equation (2.41) has to be integrated over a time step. This delivers a displacement vector (fig. 2.6) which has to be short enough that F_{DEP} does not change significant. If this is not the case the time step has to be reduced until the solution does not enhance any longer. A trajectory can then be composed out of small displacement vectors (section 3.4).

- Equation (2.29) is an expression for the force F_{DEP} on an induced dipole in a sphere. Higher order moments like quadrupoles and octopoles are for this special case neglected. Since the inducing electric field is very nonuniform compared to the size of the particles we have to expect multipolar moments [JW96, WJ96]. In [VBT$^+$01] an attractive iterative calculation algorithm for DEP forces was presented which could in principle be used for this model but it would introduce an increase of computing power and complexity. Our model can be seen as a first order estimation for showing the principle behavior of the device.

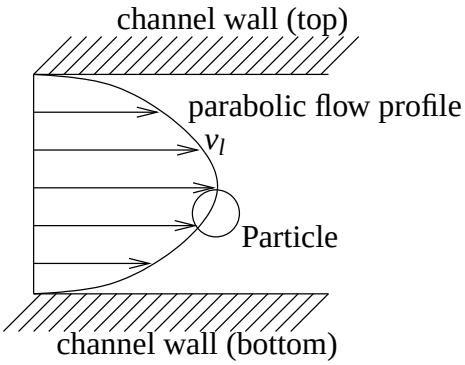

Figure 2.5: Particle in a parabolic flow. For the calculation of the drag force in the model the liquid velocity v_l in the center of the particle is used.

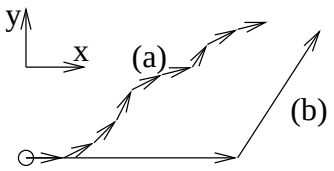

Figure 2.6: Particle trajectories for different integration time steps. (a) shows a better trajectory than (b) because of a shorter integration time. One arrow indicates one integral solution of equation (2.41).

Chapter 3

Simulation

3.1 Introduction

In this chapter the development of a two-dimensional model for a flow channel with electrodes for dielectrophoresis is explained. The model was needed for the optimization of the channel geometry and the electrode design. First a FEM electric field and a fluid flow simulation using *Coventorware* is described (sections 3.2 and 3.3). This data is fed into a *Matlab* model (section 3.4) which allows for a parametric study of the device.

3.2 FEM electric field simulation

For the calculation of the electric field distribution in the channel it is sufficient to formulate the problem as a two dimensional electrostatic potential problem. No space charge has to be taken into account and the boundary conditions are given at the electrodes. Thus the so called *Laplace Equation*

$$\nabla^2 \Phi = 0 \tag{3.1}$$

has to be solved, where Φ is the electrostatic potential. This can in principle be done analytically by finding a solution to eq. 3.1 and adapting it to the special boundary conditions or by means of a finite element solver. For this simulation the FEM solver from *Coventorware* was used which has the advantage, that it can also process fluidic simulations.

The electrode structure of the device consists of elements (DEP actuators) which are assembled to a periodic array (fig. 3.1). Therefore it makes sense to simulate the electric field for a part of the channel and use this results for composing the field distribution for the full channel in the model. So the amount of data can be reduced significantly.

In fact a larger section containing two DEP actuators was simulated, and a smaller section was cut out and used in the model. It was necessary to simulate a larger part, because there are boundary effects which influence the simulation result in the center.

The following work flow outlines the necessary steps for the simulation:

- Generate a process file. For a two dimensional simulation the process does not reflect a real process flow. Instead the device process has to be defined such that the masks show the device from a side view (and not from the top view). Table 3.1 shows the process steps.

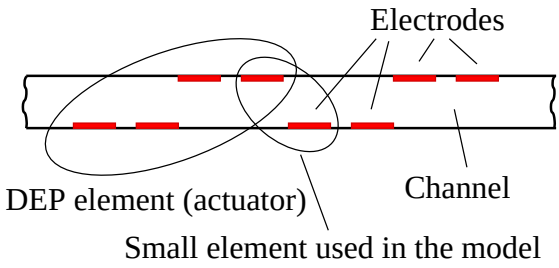

Figure 3.1: The device consists of a periodic array of DEP elements (actuators). For the simulation of the electric field distribution only two such elements (consisting of e.g. four electrodes) are used. In the model a small section of this simulation is merged several times to get a large matrix.

Action	Type	Layer Name	Material	Thickness	Mask Name / Polarity	Depth
Base		Substrate	SILICON	50	GND	
Deposit	Planar	Layer1	WATER	1000		
Etch	Front, Last Layer				channel +	1000
Etch	Front, Last Layer				electrodes -	1000

Table 3.1: Process steps for the electric field simulation.

- Generate a mask layout with the designer. As already mentioned, it is necessary to design the device from the side view. Thus these masks do not reflect the masks as they would be used in a real process. The design looks like in figure 3.1 where the electrode mask is red (grey) and the channel mask is black colored.
- Generate the model/mesh in the preprocessor. For a faster simulation only a water layer is used in the model (the electrodes are not existent, not even in the process). The boundary conditions are directly applied to the interfaces on the WATER layer. Manhattan bricks with a size of $2 * 2\mu m$ were defined in order to have an easy to use mesh for further processing[1]. Only at the electrode edge regions the mesh elements are smaller due to the given electrode height of $300nm$ (fig. 3.2).
- Finally the simulation has to be carried out. The result is shown in figure 3.3. It has to be exported to a common readable format (ASCII Tecplot) containing mesh and electric field information. From there it is converted to a *Matlab* readable file using a custom made *Perl* script. (link to appendix follows)

3.3 FEM fluid flow simulation

The velocity distribution of a fluid in a channel is governed by the Navier Stokes equations containing mass momentum and energy conservation [Whi01]. In *coventorware* a three dimensional model of the channel was designed in order to evaluate the velocity distribution of the

[1]This simulation data is fed into the matlab model of the channel. Therefore a well defined mesh geometry has to be used.

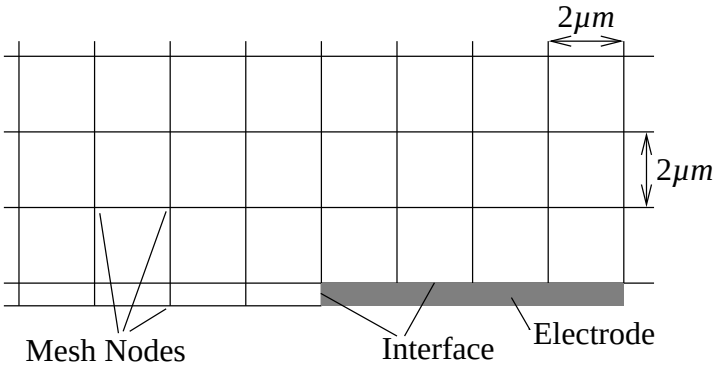

Figure 3.2: Mesh at the boundary between electrode and water. The electrode (grey) at the lower right side does not exist in the model. The boundary conditions (voltage) are applied directly to the interface at the water layer. Thus a metal (electrode) layer in not required for the simulation. Due to the small height of the electrodes the lowermost mesh elements do not have the same size as the other elements. Since this can cause trouble when the gradient is calculated these elements are cut away in the matlab model.

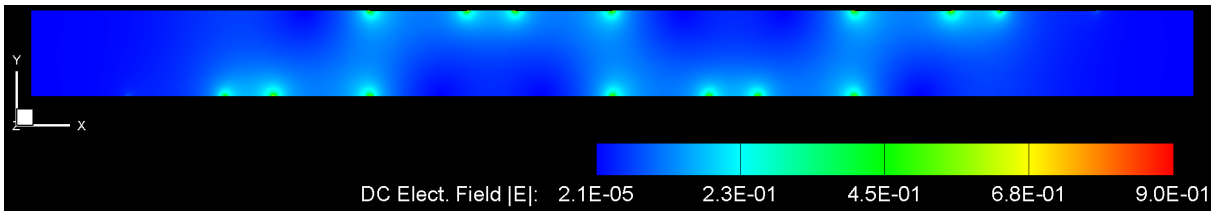

Figure 3.3: Result of the electric field simulation using coventorware. The brighter (green) areas are regions of higher electric field strength and are located between neighboring electrodes. Note that this illustration shows the absolute value of the electric field. For the DEP force generation the gradient of this field is responsible.

Action	Type	Layer Name	Material	Thickness	Mask Name / Polarity	Depth
Base		Substrate	SILICON	50	GND	
Deposit	Planar	Layer1	WATER	70		
Etch	Front, Last Layer				channel +	70

Table 3.2: Process steps for the fluid flow simulation.

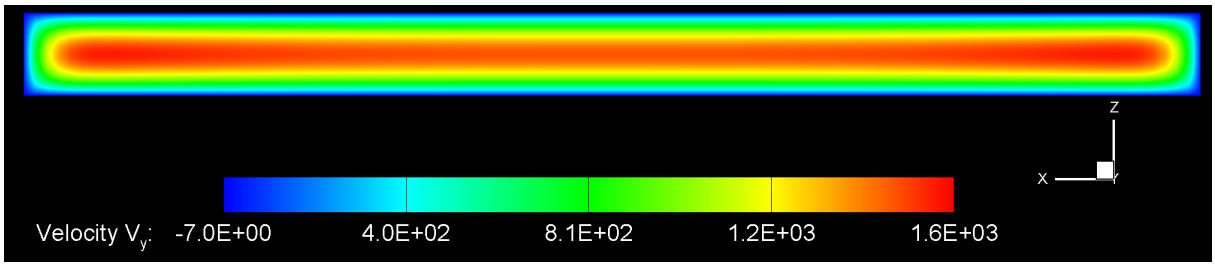

Figure 3.4: Result of the fluid flow simulation using coventorware. The figure shows the velocity distribution in a slide abeam to the flow direction. A velocity of $1 mm/sec$ at the inlet face was assigned as the boundary condition. If different flow rates are desired the profile can be scaled linearly.

fluid in the channel. The work flow is similar to that of section 3.2, except that the masks have to be designed from the top view (like for a real process). Table 3.2 shows this process. In this simulation we are interested in the vertical and horizontal flow profile for a well developed flow. Thus the resolution in the plane transversal to the flow must be high, while in flow direction a lower resolution is sufficient. The channel length has to be long enough[2] to ensure a fully developed profile. An example for a results of this simulation are shown in figure 3.4 and 3.5.

3.4 2D model of the device

For the development of the device it is essential to have a model which allows for a parametric study of its behavior. Therefore a matlab model was developed which uses the electric field distribution, the fluid velocity distribution, the channel geometry and the particle size as input. Then a particle trajectory and the retention time of a particle in the device are calculated.

If the channel geometry and the electric field distribution are fixed, two parameters can be adjusted in order to optimize the result. The voltage factor scales the applied voltage at the electrodes and the velocity factor is responsible for the fluid velocity scale. This is possible because the field distribution in both cases is independent form the appropriate absolute values.

The electric field simulation (section 3.2) delivers a file which includes a two-dimensional mesh with an electric field vector in each node. The matlab model reads this file into a matrix and calculates the dielectrophoretic force by applying equation (2.24) for a given particle radius. The resulting matrix now holds force information for a section of the device containing 2 DEP

[2] In the case that a constant flow rate is given as a boundary condition at the inlet, the flow develops within a few micrometers.

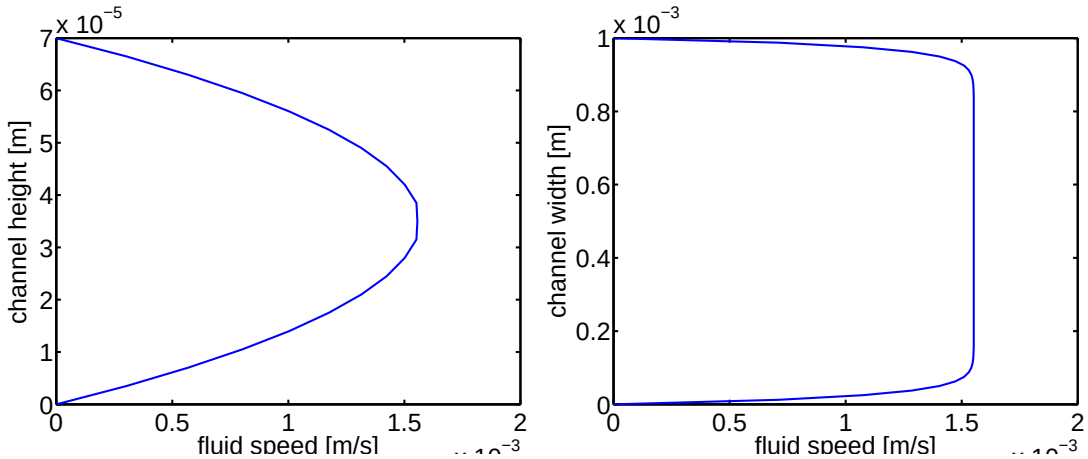

(a) (b)

Figure 3.5: For the one dimensional device simulation model only a vertical slice of the result is needed (a). (b) shows a horizontal slice of the velocity distribution used for optimizing the aspect ratio of the channel.

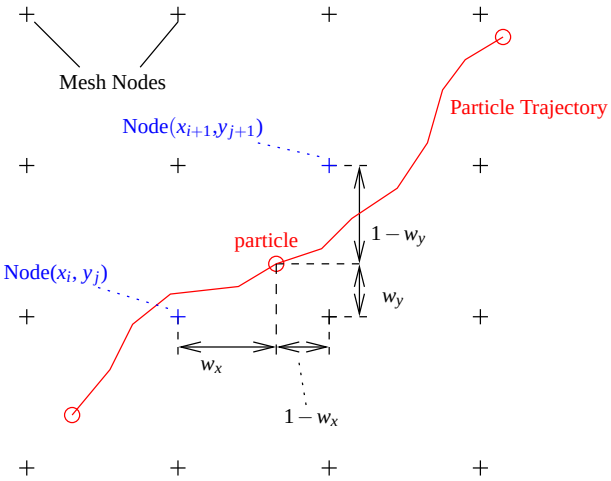

Figure 3.6: Small section of the mesh. w_x and w_y are the weights that are used to calculate the linear mean value of the force and velocity respectively. The particle trajectory consists of small even lines representing a solution of equation (2.41) each.

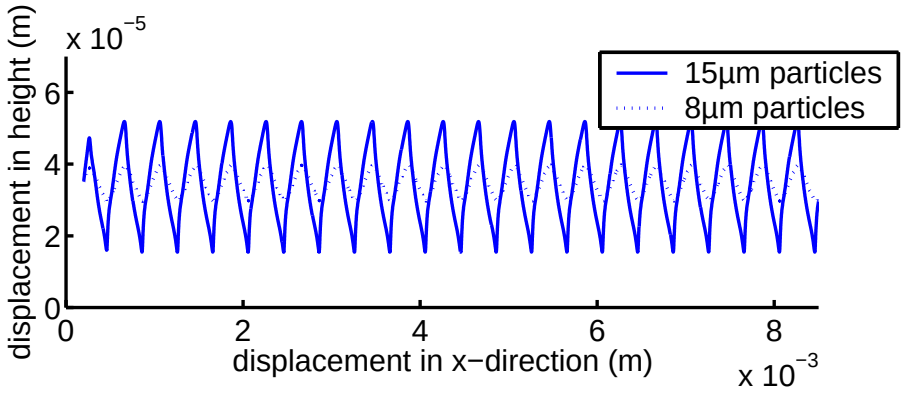

Figure 3.7: Particle trajectories for different particle sizes.

elements (see figure 3.1). Now a large matrix representing the full channel is composed of small elements containing two electrodes each (see fig. 3.1).

The result of the fluid flow simulation (section 3.3) is also imported by the model. So all necessary information for solving equation (2.41) is available. The two components (x,y) of the velocity of the particle can be calculated and the integration of this delivers directly a displacement in both axis. Since the calculated velocity is constant within the integration time the calculated trajectory is a straight line (fig. 3.6). So it is obvious that the trajectory of the particle through the device has to be composed of short straight lines. The integration time can be defined in order to fix a time- and displacement resolution.

Since the DEP force and the flow velocity are only available in discrete mesh nodes a linear mean value for these quantities has to be calculated (fig. 3.6):

$$\begin{aligned} F(x,y) = &\left[F(x_i,y_j)(1-w_x)+F(x_{i+1},y_j)w_x\right](1-w_y)+ \\ &+\left[F(x_i,y_{j+1})(1-w_x)+F(x_{i+1},y_{j+1})w_x\right]w_y \end{aligned} \tag{3.2}$$

The complete listing of the matlab model and the conversion scripts can be found in the appendix (link follows).

As an example a simulation result is presented in figure 3.7 and 3.8.

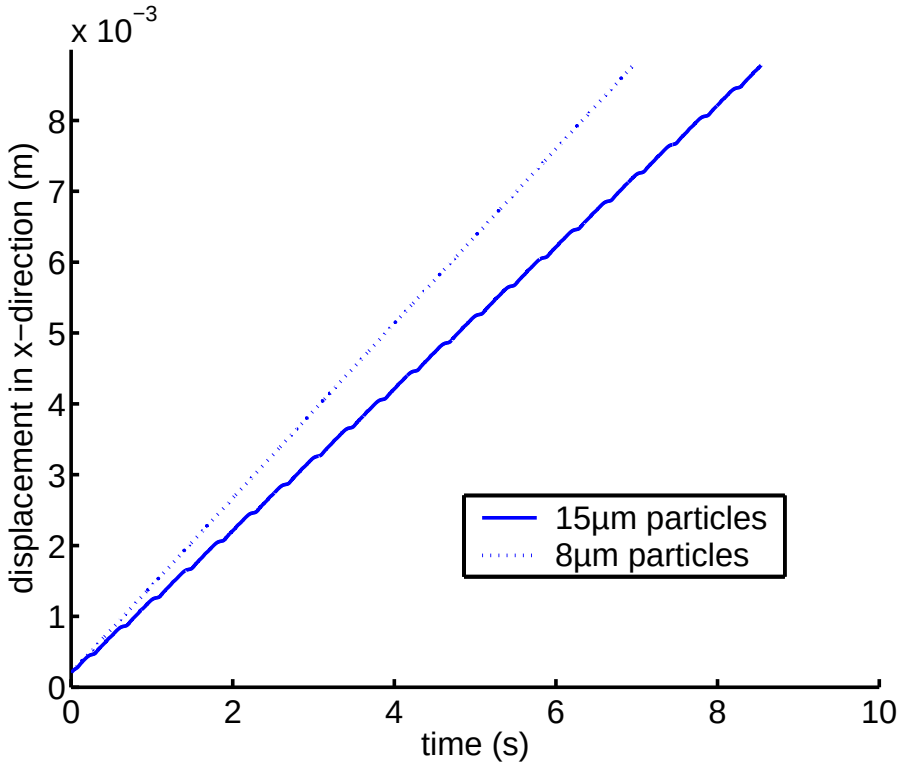

Figure 3.8: Displacement in x-direction over the time for different particle sizes. The smaller particle is faster and therefore reaches the end of the channel earlier. The stepped shape of the $15\mu m$ curve is caused by the fact that the particle is alternating between different velocities because of the parabolic flow profile combined with the vertical displacement agitation. These steps are much smaller for the $8\mu m$ particle.

Chapter 4

Device

4.1 Concept and basic description of the device

In this chapter the basic mode of operation of the device is described. The initial condition was that the device should be able to separate particles of different size. So if a sample plug is injected in the separation channel, different sized particles have to show a different retention time. For the development of the device the particle diameters were chosen between $8\mu m$ and $15\mu m$. The reason for that choice is that human blood cells are typically in this range and particles in that size can easily be observed with a microscope. If desired, another particle diameter range can be considered by scaling the whole device depending on that diameter.

Starting from this conditions the design requirements to the device are listed below:

- In order to be able to inject a particle sample plug in the channel an inlet mechanism has to be created, which forms the plug and injects it properly into the channel.
- The electrodes which are used for manipulating the particles are in direct electric connection to the liquid in the channel. In order to avoid electrolysis (bubble generation at the electrodes) it is necessary to apply AC voltages.
- In anticipation of a possible integration into a micro system the voltages are limited to a maximum of $20V$. This has a big impact on the implementation of the device. The operation principle has to be based on some kind of periodic actuation on the particles. Otherwise much higher voltages would be necessary because in a non periodic dielectrophoretic system an electric field gradient *along* the full channel length would be required in order to establish a DEP force which does not change its direction. Compared to electrophoretic systems where voltages of $2kV$ are usually applied a limitation to $20V$ makes the system cheaper and less dangerous.
- Finally the design of the device has to follow a certain scheme in order to be compatible to the existing device holder. This has to be considered when placing the inlet holes and the conduction pads. Furthermore the separation channel has to be visible when the device is clamped to the holder.

The ideas how to fulfill these requirements are presented in the following sections.

4.1.1 Separation channel

Referring to the first item of the requirements it is necessary to find a flow channel with an electrode geometry which allows for decrease of the mean particle velocity. Therefore a pressure driven flow channel which has the property of a parabolic velocity profile is used (fig. 4.1a). So particles are exposed to different liquid velocities depending on their vertical position in the channel.

Since the dielectrophoretic force strongly depends on the particle diameter it can be used to bring different sized particles to the desired vertical position.

The channel has a length of approximately $1cm$ as a result from the device holder dimensions. A small difference in the mass density between particle and liquid material would cause a buoyancy or gravity force and the particle would not stay on the initial height while passing the channel. After a few millimeters it would settle on the top or bottom of the channel. Therefore dielectrophoretic forces are an attractive possibility to keep them on track. These forces are used to move the particles up and down in vertical direction (fig. 4.1b). They are forced on trajectories with amplitudes depending on their diameter (fig 4.1b) because of the diameter dependency of the dielectrophoretic force.

Larger particles will have a larger amplitude and therefore a longer retention time in the channel. When particles of different size are injected at the same start time a separation should be established at the end of the channel.

In order to find an optimal electrode structure different types have been simulated and their operation efficiency was compared (section 4.2.3).

4.1.2 Sample injection

In literature different injection schemes for micro channels can be found [SKKW02]. A very important one is the cross flow injection, where a flow carrying the particles and another flow representing the sheath liquid pass a crossing in the device. Sample plugs can be formed by switching these flows on and off. A big disadvantage of such a system is that at least two pumps and extremely precise valves are necessary for switching these small volumes. Additionally switches in the fluidic system could introduce pressure peaks and disturbances of the velocity. This can have a direct impact on the time measurements.

In order to avoid these problems, it was considered to use dielectrophoretic forces to manipulate only the particles and not the liquid. So only one constant liquid flow carrying all the particles is necessary and the DEP forces are used to stop these particles in the drag flow (fig. 4.2). Only one pump and no valves are required and the injection can be controlled fully electrically.

For stopping the particles in the flow very high electric field gradients are necessary. At a given voltage and particle diameter there exists an upper limit for the channel height such that the particles can be trapped safely.

If the second trap is also active and the first one is deactivated for a short period of time, a few particles move from the first trap to the region between the two traps (particle 2 in figure 4.2). So particles can be accumulated and released in small portions.

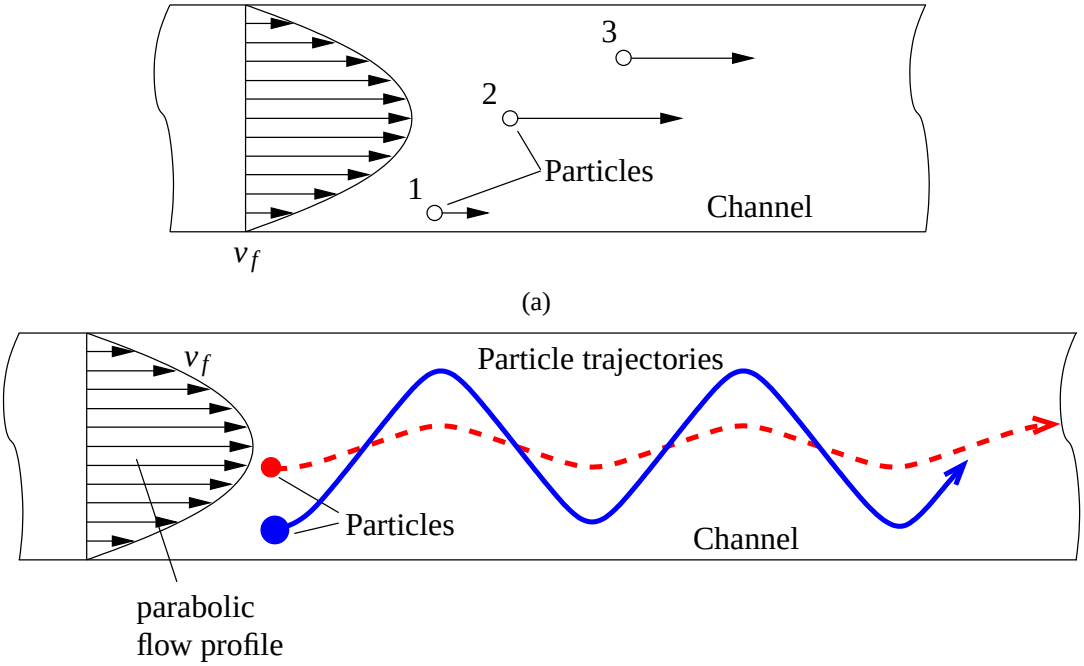

Figure 4.1: Particles exposed to a pressure driven flow in a separation channel. (a) Due to the parabolic velocity profile of a pressure driven flow, the horizontal velocity v_f (arrows) depends on the vertical position. So particles travel with different velocities depending on their vertical displacement. The disadvantage of such a channel is that a small buoyancy force would additionally move the particles up or down and therefore the initial vertical displacement would get lost. (b) An improved structure was found where a difference in the mean velocity can be achieved by forcing the particles on certain trajectories by means of dielectrophoretic forces. Larger particles, for which these DEP forces are stronger, show a higher trajectory amplitude and therefore a longer retention time.

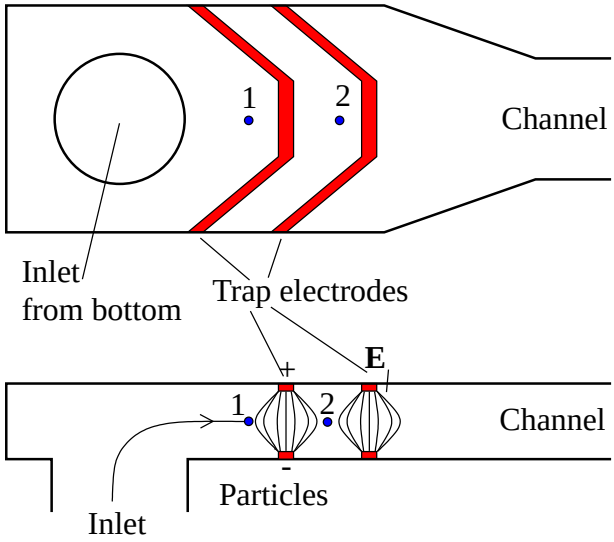

Figure 4.2: Top and side view of the double trap injection system. The liquid containing particles is pumped through the inlet. The particles can be accumulated at the dielectrophoretic traps (1 and 2) and be released in small portions.

4.2 Design considerations

There are different properties of the device which have to be considered:

- The *channel height* has to be fixed between two boundaries. The upper boundary is given by the *trap structure* where the smaller particles (diameter of $8\mu m$) have to be trapped with an electrode voltage of $20V$ maximum. The lower boundary is determined by the maximum particle diameter ($15\mu m$) for which blockage effects should not occur.
- The *aspect ratio* of the channel cross section is selected such that a flat horizontal velocity profile is established in the channel. So distributed particles at the same vertical position are exposed to the same liquid velocity.
- A *principle electrode structure (DEP actuator)* is found by comparing different designs with respect to their efficiency.
- The *electrode dimensions* are then optimized in a last step.

In the following sections these items are discussed in detail.

4.2.1 Channel height and DEP trap

As already discussed, a dielectrophoretic trap structure is used as an injection facility. The dielectrophoretic forces which are necessary to stop the particles in the liquid can be expected to be much stronger than the forces in the separation channel where the particles only have to be displaced. In this section it will turn out that the trapping condition for the small particles is responsible for the maximum allowed channel height.

When a particle comes to the region in front of the first trap (fig. 4.2 particle 1) it is stopped due to the force balance between dielectrophoretic and drag force:

$$F_D = F_{DEP} \tag{4.1}$$

$$2\pi\varepsilon_1 R^3 K \nabla E_0^2 = 6\pi\eta R v_l. \tag{4.2}$$

For trapping the particles the squared gradient ∇E_0^2 has to be greater than the **critical value**:

$$\nabla E_0^2 > \left| 3\frac{\eta v_l}{\varepsilon_1 R^2 K} \right| = 8.8413 \cdot 10^{14} \frac{V^2}{m^3} \tag{4.3}$$

with the viscosity of water $\eta = 1.0 \cdot 10^{-3} \frac{N^2}{m^2}$, the liquid speed at the center of the channel $v_l = 1.6 \cdot 10^{-3} \frac{m}{s}$, the permittivity of water $\varepsilon_1 = 80\varepsilon_0$, the particle diameter of the smallest particles $r = 4\mu m$ (diameter $d = 8\mu m$) and the clausius mosotti factor $K = \frac{\varepsilon_2 - \varepsilon_1}{\varepsilon_2 + 2\varepsilon_1} = -0.48$.

If the left hand side of equation (4.3) is greater than the right hand side the condition for trapping is fulfilled. This trapping condition depends on 3 different items:

- The absolute value of the electric field depends linearly on the inverse channel height $\frac{1}{h}$ (with constant voltage). Therefore we can assume that

$$\nabla E^2 \backsim \frac{1}{h^2}. \tag{4.4}$$

- The drag force F_D scales linearly with the liquid velocity:

$$F_D \backsim v_l \tag{4.5}$$

- The dielectrophoretic force scales quadratic with the applied voltage:

$$F_{DEP} \backsim U^2 \tag{4.6}$$
$$\nabla E_0^2 \backsim U^2 \tag{4.7}$$

Now two scaling factors are introduced which are sufficient in order to show the impact of these three items on the trapping condition (eq. (4.8)). The first factor (f_1) scales the electric field E_0 and the other one (f_v) is responsible for the liquid velocity.

Using this factors the trapping condition can be formulated as

$$f_1^2 \nabla E_0^2 > 3 f_v \frac{\eta v_l}{\varepsilon_0 R^2 K} \tag{4.8}$$

In figure 4.3 the dependency between the trapping condition and the two factors is illustrated. With the electric field simulation of the trap electrode structure of a given channel height of $70\mu m$ this condition is illustrated in the form that f_1 is a function of f_v (fig. 4.3).

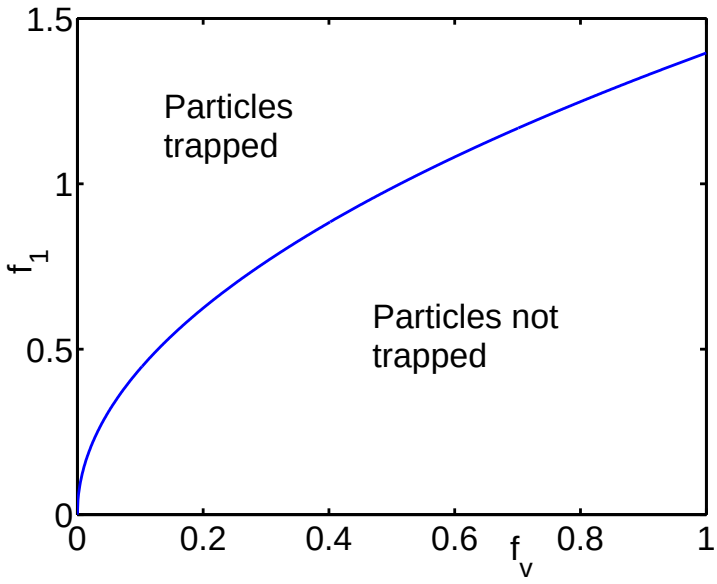

Figure 4.3: Scaling factors for the operation of the trap. The line represents the trapping condition (critical values). f_1 scales the electric field and f_v scales the velocity. Particles are trapped in the area above the line. This graph is valid for $8\mu m$ particles at a liquid velocity of $v_f = 1.6\frac{mm}{sec}$ and a applied voltage of $U = 10V$ in a $70\mu m$ channel. The trap has to be dimensioned for the smallest allowed diameter. Larger particles ($15\mu m$) can be trapped with a much smaller voltage (see eq. (4.2)).

The maximum of ∇E^2 for this simulation (particle diameter $8\mu m$, liquid velocity $v_l = 1.6\frac{mm}{s}$) is $4.5389 \cdot 10^{14}$ which is not enough for trapping $8\mu m$ particles if $f_1 = f_v = 1$ (see eq. (4.8) and

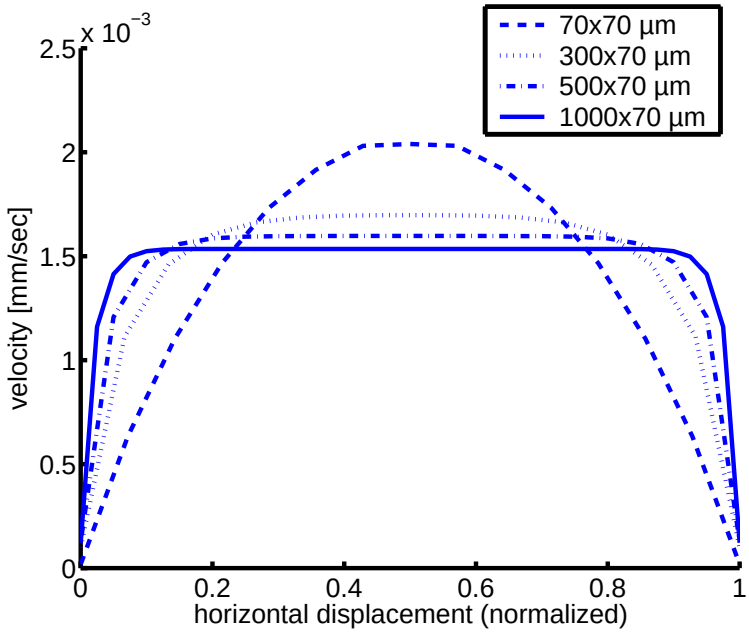

Figure 4.4: Horizontal velocity profile over normalized channel displacement for different aspect ratios. At a ratio of $\frac{1000}{70}$ the profile is flat in nearly 80% of the channel.

fig. 4.3). Broadening the channel such that $f_v = 0.5$ and increasing the voltage (or decreasing the channel height) moves the operation point to the safe area.

The decision for a specific channel height is a tradeoff between the maximum field strength at the electrode edges and the lowest acceptable ratio between channel height and particle diameter. This ratio is important for the estimation of blockage effects in the flow.

We selected a height of $70\mu m$. The ratio between particle diameter and channel height is therefore $\frac{70\mu m}{15\mu m} = 4.7$. So the necessary voltages for trapping are well below 15V.

4.2.2 Aspect ratio of the channel cross section

In the common operation mode of the device a number of particles should be processed at the same time. A sample containing these particles is injected and so the cross section of the channel has to have a certain area such that the particles do not disturb each other. The idea is that particles which are traveling at the same vertical displacement but beside each other are exposed to the same liquid velocity. This can be achieved by choosing the aspect ratio such that the horizontal flow profile is flat shaped in a large part of the channel. Figure 4.4 shows the simulation of the horizontal flow profiles for channels with different aspect ratios. With increasing channel width the region of flat velocity profile grows. An aspect ratio of $\frac{1000}{70}$ enables the usage of approximately 80 % of the channel width. Therefore it was decided to choose a channel width of $1000\mu m$.

Note that the vertical flow profile should stay parabolic in order to keep the functionality (see fig. 4.1).

The determination of the aspect ratio is also affected by possible blockage effects which appear if the ratio between particle diameter and channel diameter reaches a certain value [BE02].

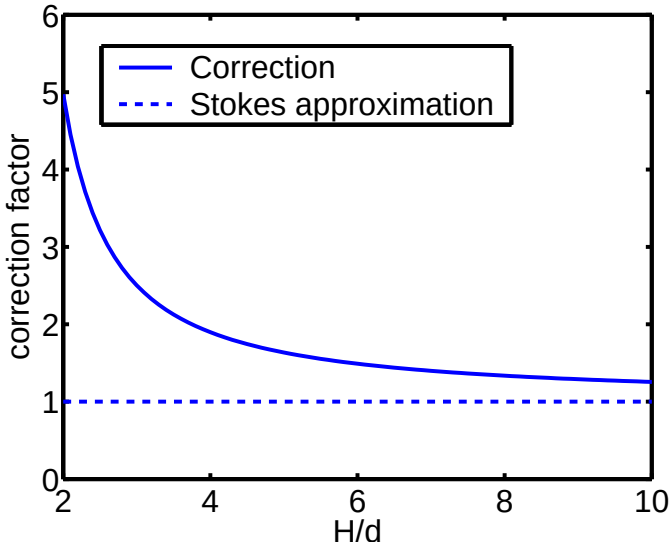

Figure 4.5: Correction factor for the drag force on a particle in a blocked channel. H/d is the ratio between the diameters of the pipe and the particle.

In literature the case of a sphere (diameter d) in a circular shaped pipe (diameter H) is often discussed. For this case figure 4.5 shows the correction factor for the drag force approximation (eq. (2.25)) which is taken out of [BE02].

At a ratio of $\frac{H}{d} = 5$ the stokes drag law and therefore the drag coefficient has to be corrected by a factor of approximately 1.5.

At a channel height of $70\mu m$ this ratio is $\frac{H}{d} = 4.7$ but the shape of the channel in our case is rectangular and not circular. Furthermore with an aspect ratio of $\frac{1000}{70}$ we can estimate that the multiplicative factor for the drag coefficient will be well below 1.5 and the Stokes drag formula is valid for our channel.

4.2.3 Principle electrode structure (DEP actuator)

For moving the particles up and down a periodic electrode structure on top and bottom of the channel is required. Therefore, a principle electrode structure called DEP actuator had to be found which fits for the task of displacing the particle a to certain height.

Three different designs were considered (fig. 4.6). For these designs a simulation as described in section 3.4 was carried out and the output was compared. The optimization variable was the maximum displacement a particle would reach in each structure under same conditions. The simulation results (trajectories) for the three different approaches are shown in figure 4.7.

The structure with one electrode on top an bottom (fig. 4.6a) shows a poor vertical displacement (fig. 4.7). The second type (fig. 4.6b) shows a much better result. So it seems that the electric field between the bottom electrodes is responsible for the slope of the trajectory. The strong gradient there pushes the particle toward the top of the channel. Additional electrodes on top and bottom (fig. 4.6c) improve the result, but do not change the slope of the trajectory (dotted line in fig. 4.7).

It can be shown that the retention time is independent of the spacial trajectory period if

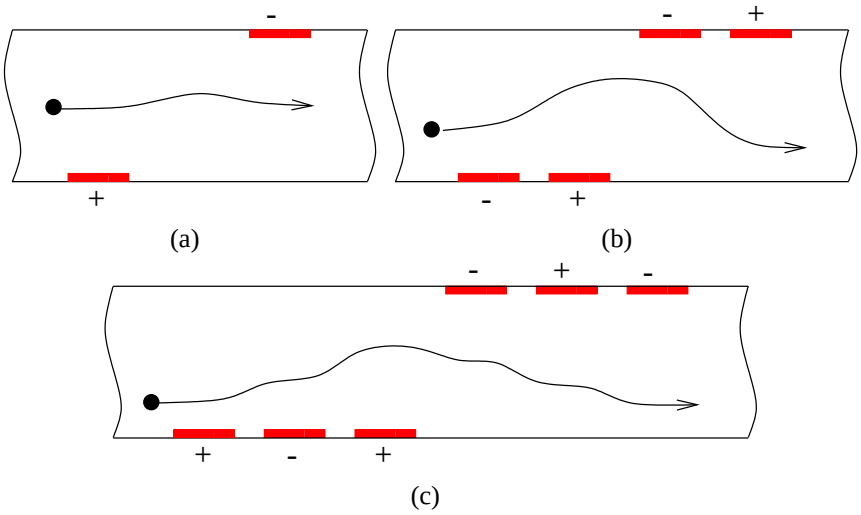

Figure 4.6: Three different DEP actuator geometries

the same amplitude is taken as a basis (fig. 4.8). If more electrodes are used (and therefore the period is larger) a smaller dielectrophoretic force is sufficient to reach the same amplitude because the particle is exposed to that force for a longer time. So the decision whether to use more or less electrodes can be seen as a decision between higher or lower dielectrophoretic forces (if the same vertical displacement is desired). A higher DEP force has the advantage of being more dominant compared to gravity or buoyancy forces in the system.

Simulation showed that there exists an upper limit for the trajectory amplitude which is determined by the fact that particles are trapped if they reach a region too near to the electrodes. This means that the maximum amplitude is limited. When this limit is crossed trapping may occur.

Considering the advantage of the more dominant DEP forces and the fact that it is possible to reach the same amplitudes with both structures (4.6 a and b) we decided to use the design with four electrodes shown in figure 4.6b for the further considerations.

If desired with this actuator it is possible to push particles against the top or bottom of the channel.

4.2.4 Electrode dimensions

Now the principle actuator structure is selected and so an optimization of its dimensions (fig. 4.9) can be carried out. Therefore the electrode width w and the spacing between the electrodes g (gap) was varied and the reachable vertical displacement for a particle was observed. Figure 4.10 shows the results for three different electrode widths. At a voltage of $U = 10V$ and an initial start displacement of $50\mu m$ the maximum displacement for a $10\mu m$ particle is shown. This analysis shows, that the optimum gap gets smaller when the electrode width raises. Therefore the more common conclusion can be drawn that the overall length of one electrode plus gap **(pitch) is an important measure for the optimum** (in all three series of simulations in figure 4.10 the maximum height is achieved with a pitch of $120\mu m$).

The best results were obtained with an electrode width of $80\mu m$ for a channel height of $100\mu m$. For the realized device a channel height of $70\mu m$ was chosen and therefore it can be

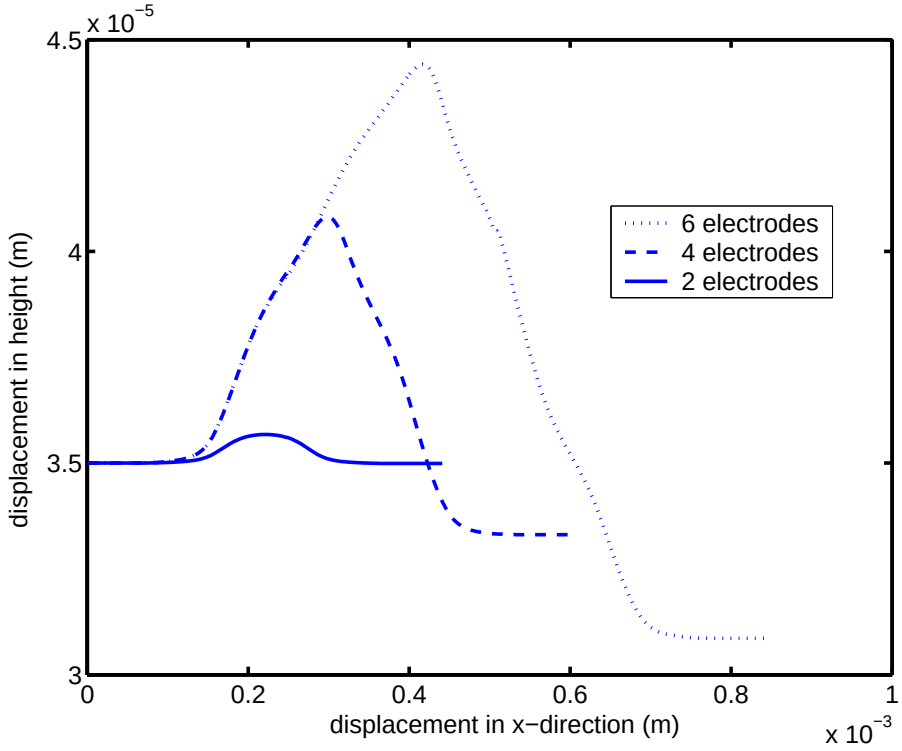

Figure 4.7: Simulated particle trajectories for the three different actuator structures shown in figure 4.6a, b and c. Voltage $U = 3.16V$, particle diameter $d = 10\mu m$ and channel height $h = 70\mu m$

assumed that the result would enhance because the DEP forces in this case would be stronger. However, this optimization was not repeated for the smaller channel height because much numerical simulations are involved and the result was estimated to be better.

Since the ideal electrode geometry for one DEP actuator is given by the last simulation ($w = 80\mu m$, $g = 40\mu m$) the question arises in which pitch these actuators should be placed in the channel. Therefore the model derived in section 3.4 can be utilized. Beside the particle trajectory it delivers the retention time in the channel. The comparison of this value for large and small particles gives an optimization quantity. The results are shown in table 4.1. This

d in μm	-20	0	100	200	400
$\frac{\Delta t}{t_0}$ in %	14	15.5	8.26	7.2	6.2

Table 4.1: Retention time differences in percent for large ($15\mu m$) and small ($8\mu m$) particles for different d (distance between actuator elements).

shows that a value of $d = 0\mu m$ gives the best result in retention time difference. So the following dimensions were finally taken for the DEP elements: $w = 80\mu m$, g=$40\mu m$, $d = 0\mu m$.

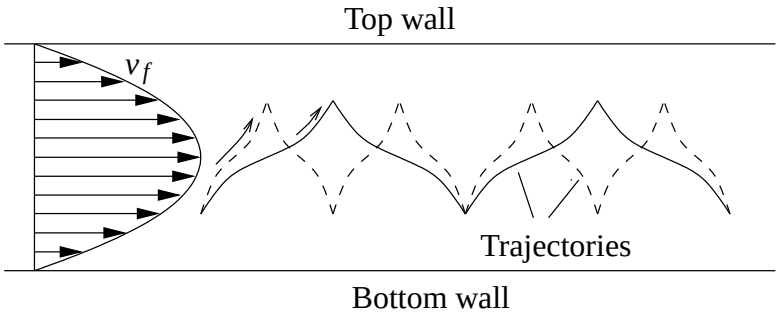

Figure 4.8: Two particle trajectories with the same amplitude but different spatial period. It can be shown that both have the same retention time in a channel with a parabolic flow profile. A smaller dielectrophoretic force is necessary for the larger period because the particle is exposed to it for a longer time.

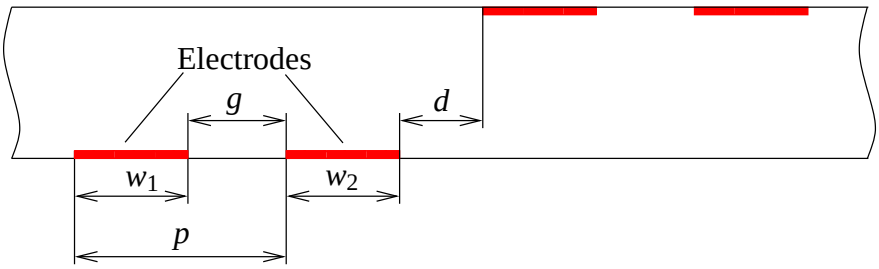

Figure 4.9: Dimensions of the actuator to be optimized. w_1,w_2...Electrode widths, g...spacing between electrodes (gap), d...spacing between the actuators. Only the case of $w_1 = w_2 = w$ was considered.

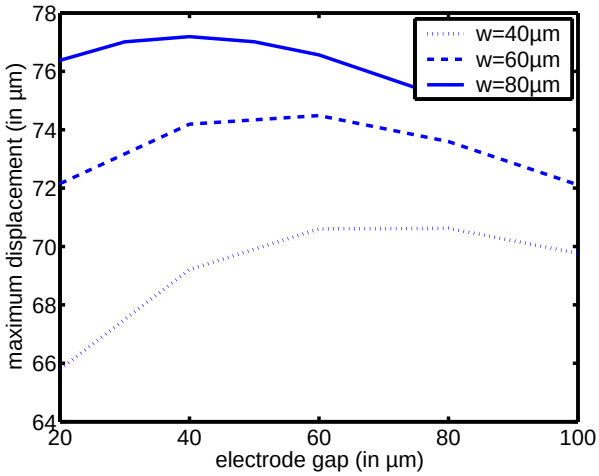

Figure 4.10: Maximum reachable displacement for a $10\mu m$ particle as a function of the spacing between the electrodes for different electrode widths (40, 60 and 80 μm). The initial displacement is $50\mu m$ and the applied voltage is $U = 10V$. Channel height $h = 100\mu m$

4.3 Fabrication issues

This section describes the fabrication steps for the device. First the requirements to the device are listed which yields in decisions for material and process issues. Then the process steps are discussed in detail.

At this point I have to mention that the fabrication was not part of the diploma thesis. Experts at the institute were consulted for this task. Only this expertise available at the institute made it possible to fabricate the device in the given time frame.

Nevertheless it is of importance to discuss the process since it has a big impact on the design.

Figure 4.11 shows a sectional drawing of a part of the device in order to outline the following requirements for the fabrication:

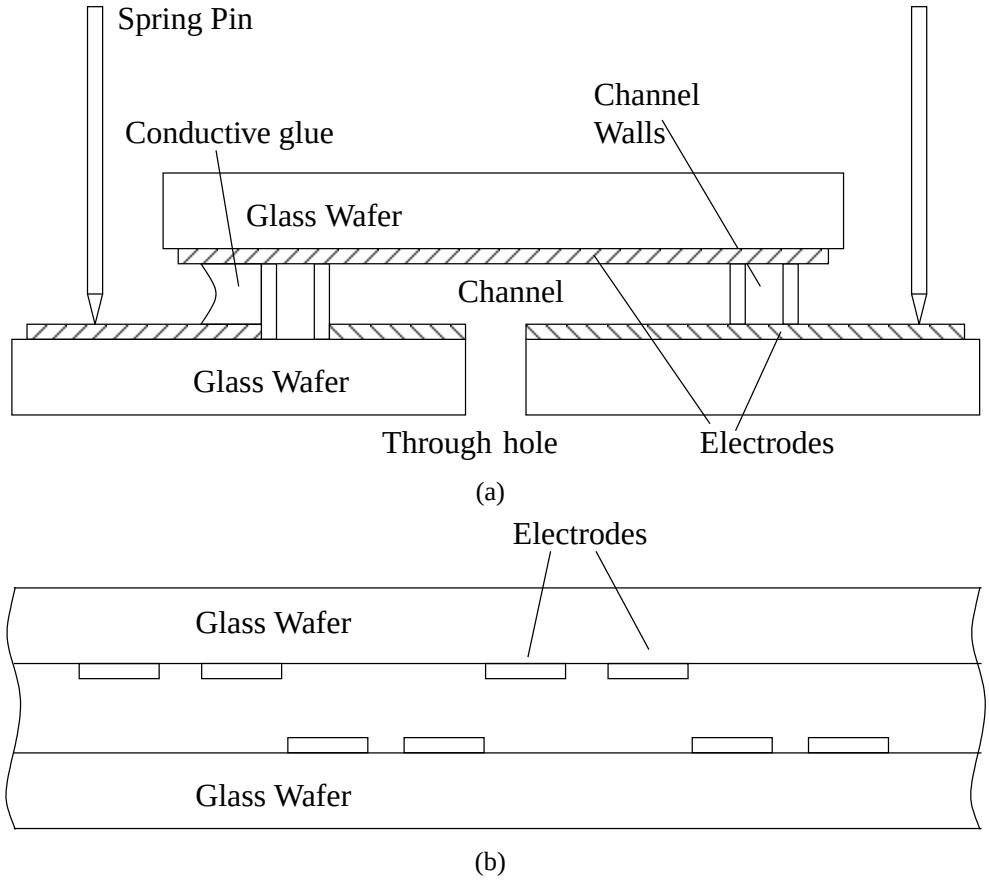

Figure 4.11: Cross section of the device. Note that the drawing is not in a correct scale. (a) Front view. The left spring pin is connected via the pad row and the conductive glue to the electrodes on the top wafer. (b) Side view.

1. The high electric field between neighboring electrodes (fig. 4.11b) requires a wafer material with high break through voltage.

2. The bottom wafer has to be equipped with through holes (fig. 4.11a) for the liquid inlet and outlet.

3. The liquid channel has to be fabricated in a precise way because the spacing between top and bottom wafer has a significant effect on the fluid mean velocity. Also the electric field in the channel is strongly depending on the channel height.

4. Electrodes have to be placed on top and bottom wafer. This demands for a precise alignment between both wafers. Furthermore the top electrodes have to be contacted to the bottom wafer where the contact pads are located.

In order to fulfill item 1 glass is the material of choice. This brings the disadvantage that the required through holes (item 2) are hard to achieve. It was necessary to contact a company which is able to deliver wafers with through holes.

As material for forming the channel the epoxy based photo resist SU-8 was chosen for the simple reason that the process is well controllable by experts within the institute [SSLV03]. In a special bonding process (described later in this section) the wafers are bonded together showing the desired accuracy.

SU-8 Structuring and bonding process As already mentioned SU-8 is the material for forming the channel structure. The process steps are illustrated in figure 4.12. The following work flow explains the process:

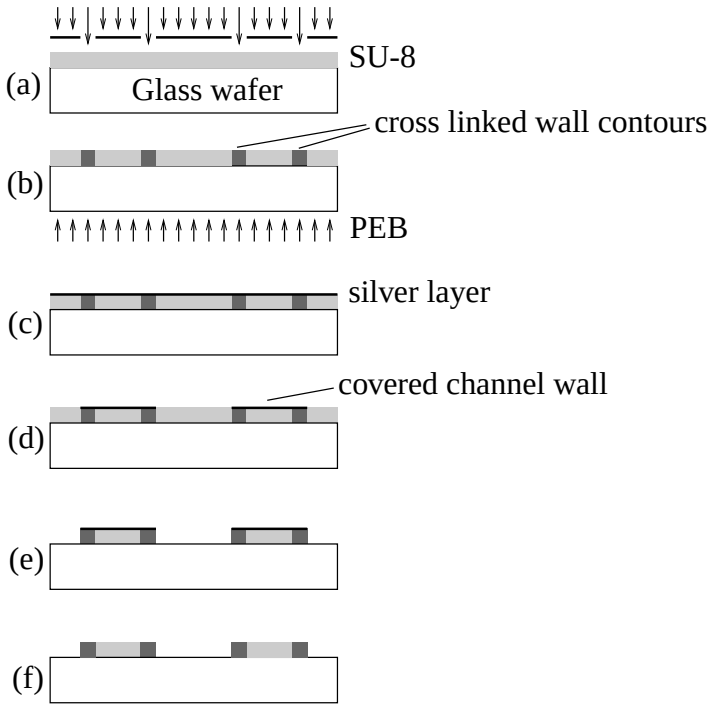

Figure 4.12: Process steps for the SU-8 pattern generation and bonding.

1. Spin SU-8 resist material on the top wafer. This is repeated several times until the desired height of the channel ($70\mu m$) is reached.

2. The wafer is exposed using the first mask containing the contours of the side walls (fig. 4.12a).

3. In a post exposure bake step (fig. 4.12b) at a temperature of $90°C$ the areas exposed in step 2 are cross linked while all other areas are not because the chosen temperature is too low for a full cross link.

4. A silver layer is now deposited which covers the full SU-8 layer (fig. 4.12c). Since in the SU-8 layer there are cross linked and non cross linked areas and the cross linked ones have a larger volume the contours of the sidewalls are visible although the SU-8 layer is fully covered by silver. This is very important for the following mask alignment. Ag is used because of its low evaporation point and therefore low radiation when heated (some areas of the SU-8 layer are still sensitive to light).

5. Then a metal patterning step is introduced by using a standard lithography method and wet etching (fig. 4.12d). Here a mask is used which covers the areas between the contours (and the contours itself). At the end of this step a silver layer is coating the channel wall areas.

6. The remaining SU-8 structure which is not covered by metal is developed and removed (fig. 4.12e).

7. The metal is removed and the wafer is ready for the bonding process (fig. 4.12f). Now a channel wall consists of unexposed SU-8 surrounded by already cross linked and thus hard SU-8.

8. In the last step the top wafer carrying the SU-8 structure is aligned to the bottom wafer using a mask aligner. A contact force of 1000 N and a temperature profile (up to 180 C) is applied to the sandwich.

At the end the wafer sandwich has to be fragmented into single devices using a saw. According to figure 4.13 a part of the top wafer has to be sawed off on order to uncover the contact pads. Then the electrodes on the top wafer are connected to the bottom pads using conductive glue (see figure 4.11a). This glue is also used to protect the pads from being damaged by the spring pins.

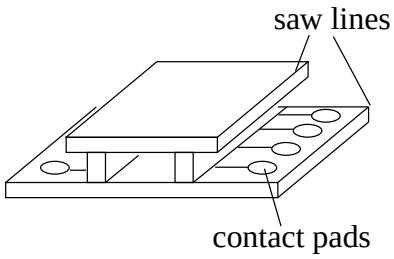

Figure 4.13: Saw lines.

4.4 Layout of the device

The design of the device has to follow some rules in order to be compatible to the existing device holder. L-Edit was used for generating the mask design. Three different designs were considered (fig 4.14):

- The main device (fig. 4.14a) consists of a bended inlet and a straight channel. The bended part was introduced in order to exploit the chip area. The active separation channel length is longer.
- The straight device (fig. 4.14b) is a backup design in the case that something would go wrong with the main device. There is no curve between inlet and separation channel. Therefore the risk of clogging is minimal. This causes a shorter separation channel.
- The serpentine device (fig. 4.14c) has a maximum channel length. In fact the separation channel is more than three times longer than the straight one. This has the disadvantage, that the channel is not continuous but consists of 3 channels separated by curves.

See figure 4.15 for images of the realized devices.

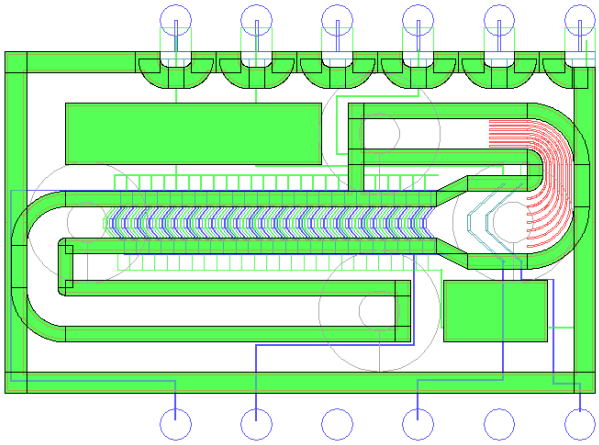

(a)

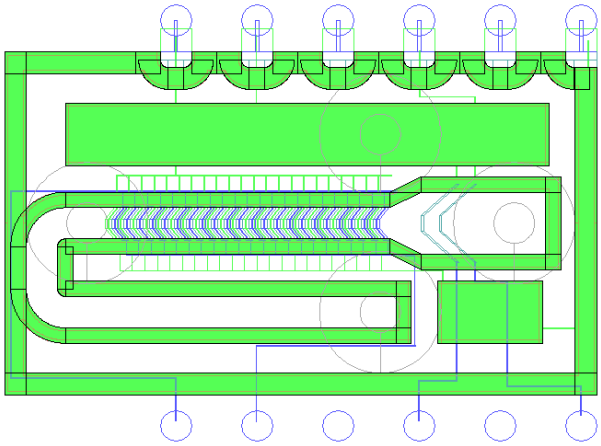

(b)

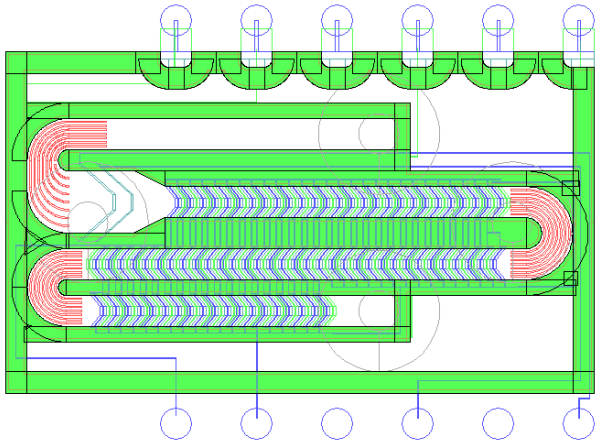

(c)

Figure 4.14: The realized designs.

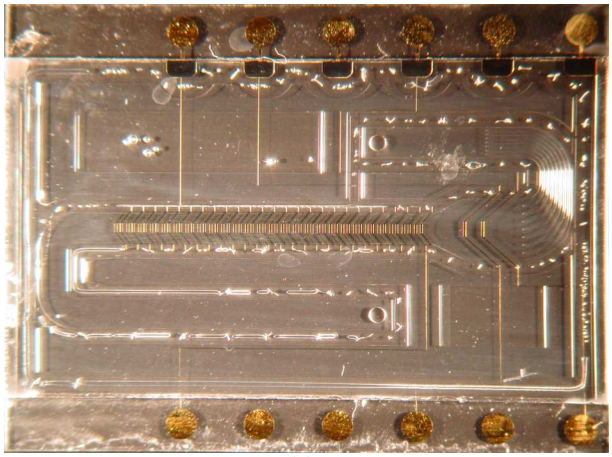

(a)

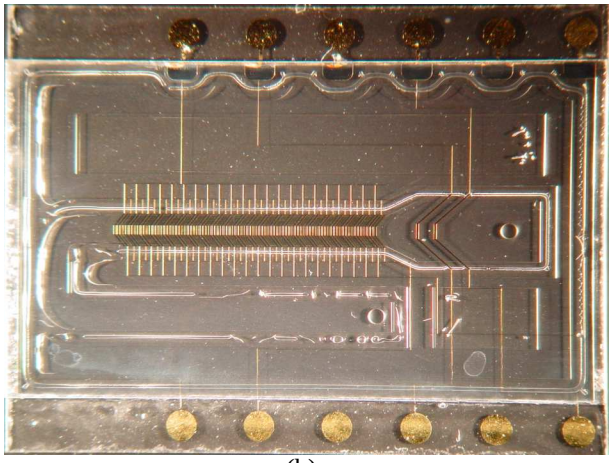

(b)

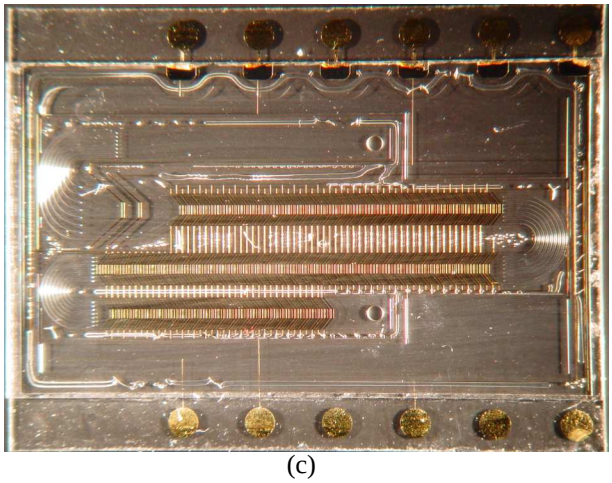

(c)

Figure 4.15: Images of the fabricated devices.

Chapter 5

Measurements

5.1 Experimental setup

Figure 5.1 shows an overview of the experimental setup. A syringe pump equipped with a magnetic stirrer was used to pump deionized water containing particles through the DEP separator chip. For controlling the double trap inlet a $1MHz$ voltage source was split up into two paths

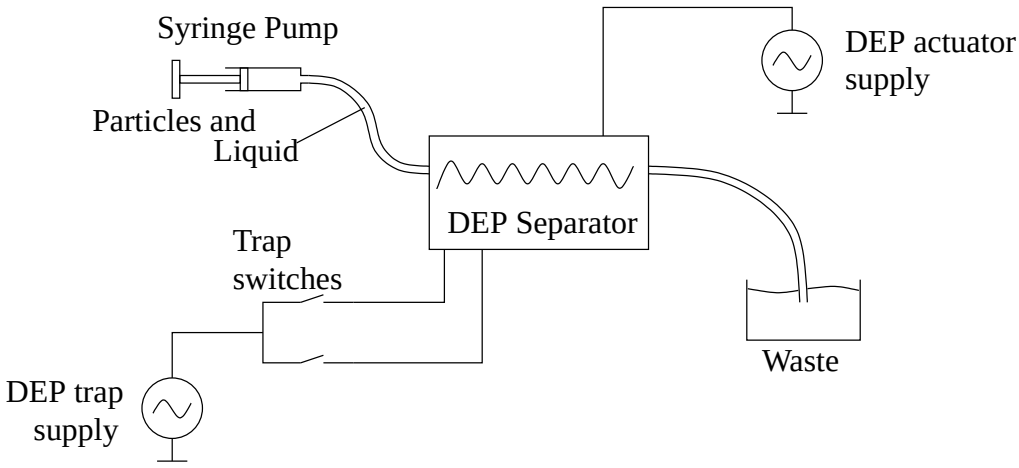

Figure 5.1: Experimental setup for the measurements. The liquid containing the particles is pumped through the separator using a syringe pump. The device has to be supplied with voltage for the trap and the separator electrodes. The traps can be activated manually.

including a switch each. So the traps could be activated manually. For the electrodes of the separation channel an additional $1MHz$ source was connected to the device.

A custom made device holder (fig. 5.2 and 5.3) was used to establish the electric and fluidic connections to the separator chip. This device holder consists of a plastic block equipped with liquid inlets for connecting flexible tubes. The chip is clamped on sealing o-rings by a transparent cover plate for establishing the fluidic connection. Spring pins are pressed against the contact pads in order to supply the chip with the electrical signals.

During operation the device was observed using a microscope. Through a milled hole in the center of the cover plate the full separation channel and trap structure can be watched. For

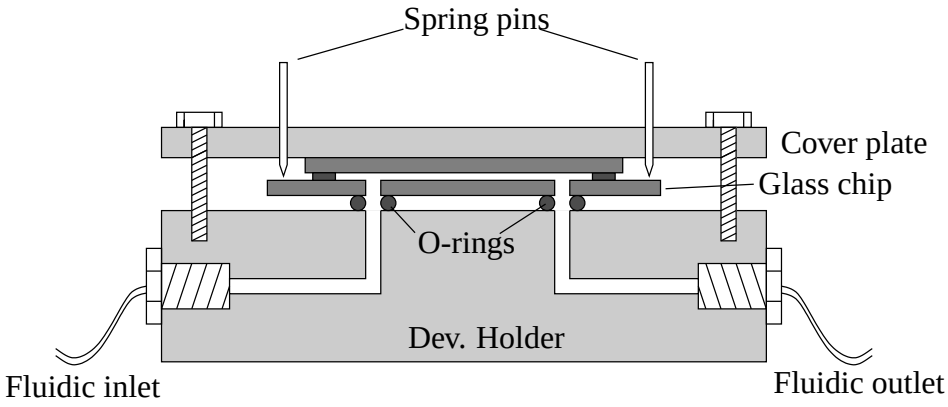

Figure 5.2: Schematic drawing of the glass chip clamped on the device holder. The chip is pressed onto the o-rings with the transparent cover plate. The fluidic connections are placed at the side of the holder. Spring pins are used to connect the device electrically.

Pump	KD Scientific, Model 200P
Syringe	Hamilton Co., Gastight®1002, 2.5ml
Particles	Micromod, micromer®-blue plain 8μm Micromod, micromer®-red plain 15μm
Microscope	Zeiss, Stemi SV 11 Apo
DEP trap supply	IEC interstate high voltage function generator F43
DEP separator supply	Good Will Instruments GFG-813
Oscilloscope	Tektronix TDS 220

Table 5.1: Used equipment and materials.

measurements the time a particles needs for passing the channel was measured manually using a computer program. The applied voltage was measured with an oscilloscope.

In table 5.1 the used equipment and materials are listed. The measurements were carried out at constant flow rates.

For the characterization of the device, measurements with two different particles sizes at the same conditions (flow rate and voltage) were carried out. It was observed that after some time the pump was running no particles were delivered any more. Since the particle material has a slightly higher density than water the upturning pipe in the device holder can be seen as a place where the particles settle. This made fast forward cycles necessary at which all the particles are flushed into the device again. It turned out that after such cycles the desired flow rate was not reached immediately. So it became necessary to follow a specific work flow (see fig. 5.4) for all the measurements in order to get comparable results.

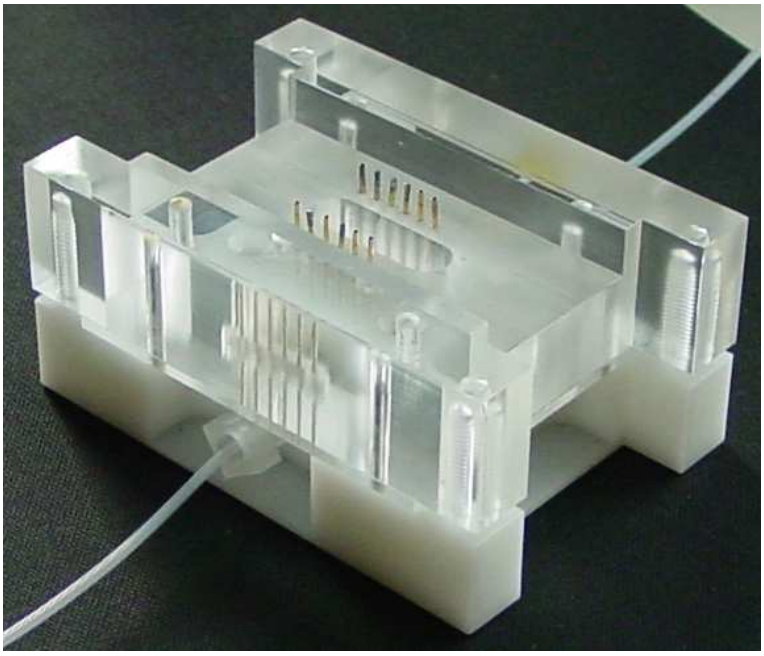

Figure 5.3: Image of the device holder.

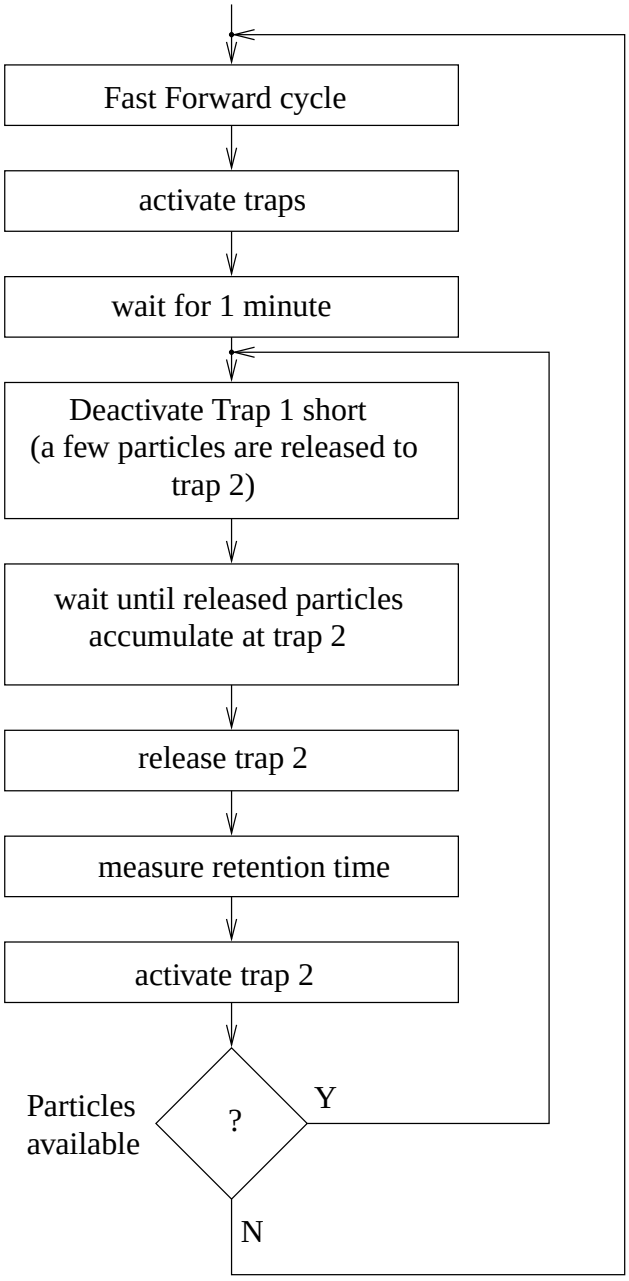

Figure 5.4: Work flow for the measurements.

5.2 Measurement results

The main goal of the measurements is to determine the retention time of particles in the channel. By supplying the electrodes with voltage there should be a noticeable change of that time.

The device also gives the possibility to verify the prediction for the dielectrophoretic and drag force. Therefore the critical voltage at which the particles are being trapped in the inlet was determined by measurements (see section C).

The results of the measurements for the separation channel are presented in the following. First the maximum voltage for the separation electrodes was determined by tuning it such that the larger ($15\mu m$) particles were just not trapped (this corresponds to the maximum trajectory amplitude). Then measurements with both particle types ($8\mu m$ and $15\mu m$) were carried out at this voltage ($5.46V$). The mean retention time for a series of 40 measurements is presented in table 5.2. The corresponding histogram is shown in figure 5.5. As mentioned above the

$\bar{t_s}$	$\bar{t_l}$	$\frac{\Delta t}{t_s} \cdot 100$ in [%]
$8.5s$	$10.6s$	24.7%

Table 5.2: Mean value of the measured retention time for $15\mu m$ (t_l) and $8\mu m$ (t_s) particles at a voltage of $5.46V$ and a flow rate of $3.5\mu l/min$. 40 measurements for each particle size.

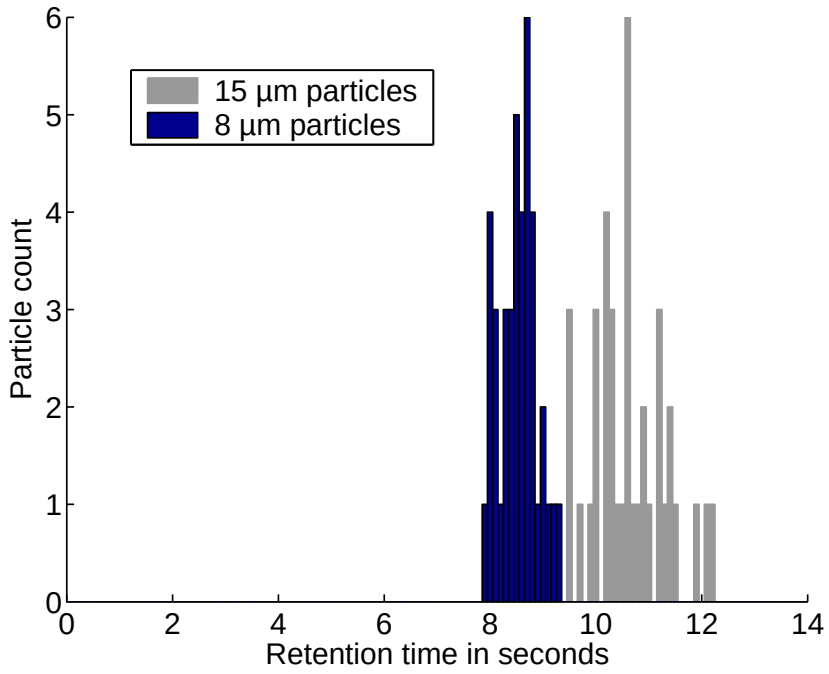

Figure 5.5: Histogram for 40 measurements per particle size at a voltage of $5.46V$ and a flow rate of $3.5\mu l/min$.

measurements were carried out for both particle types in succession. This implies a change of syringes and a restart of the pumping system. A small error in the actual flow rate affects

the measurement result integral. According to figure 5.5 the small particles show a retention time between 7.9s and 9.3s which conforms to a difference of 1.4 seconds. The reason for that difference must be found in a variation of the flow rate because simulation show that the retention time for small particles in that field range is insensitive to a radius variation (fig. 5.6).

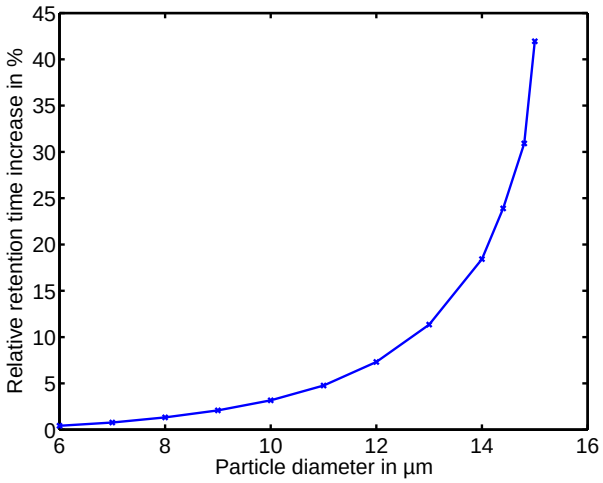

Figure 5.6: Simulated relative retention time in % over particle radius for $U = 4.43V$. The retention time shows a much higher sensitivity to the particle size for larger particles.

The larger variation of the retention time for $15\mu m$ particles can be found in the much higher sensitivity compared to smaller particles (fig. 5.6). A slightly different particle radius influences the retention time dramatically. This very high sensitivity brings up the possibility to use this device as a sensor for measuring the particle diameter.

5.3 Interpretation

The results presented above can be used to verify the theoretical model. Therefore the model was used to find the voltage at which the relative retention time matches with the one of the measurements.

Compared to the voltage used in the model (4.43V) a 23.3% higher voltage (5.46V) is necessary for establishing the same retention time difference (24.7%) in the fabricated device. This significant mismatch between model and measurements is a product of the neglection of higher order moments in the dielectrophoretic force calculation of the model.

In [VBT$^+$01] a dielectrophoretic trap was investigated where higher order moments play a significant role. The calculation (based on [JW96] and [WJ96]) shows a remarkable decrease of the dielectrophoretic forces at higher voltages. In fact the derivatives of the electric field gradient within a characteristic length (particle diameter) are responsible for additional forces. All dielectrophoretic forces (first and higher order) scale quadratic with the applied voltage and therefore higher order moments which can be neglected for small voltage appear much stronger with increased voltage.

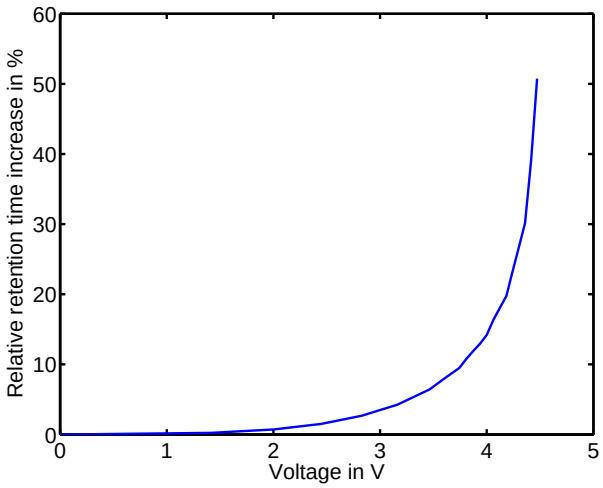

Figure 5.7: Relative retention time increase over applied voltage. For 24.7% retention time increase a voltage of $4.43V$ is required for $15\mu m$ particles.

Chapter 6

Discussion

In this section some practical issues concerning the project are discussed. First the separation efficiency is defined and the obtained results are assessed (sec. 6.1). As already mentioned in 5.2 the retention time measurements were carried out manually using a stopwatch program. So the measured values can be expected to be loaded with an error introduced by the response time of the operator. The results presented in 5.2 can therefore be interpreted as being adequate to proof the principle.

For a better quality of the data an automatic detection system would have to be added. Section 6.3 gives some suggestions for a possible detection system.

In the experiments it turned out that the sample injection has some room for improvements. This issue is addressed in section 6.2.

6.1 Separation efficiency

In this document the term separation efficiency is defined as the retention time difference between separated particles in percent. For a characterization of the device the retention time was measured for different particle sizes. This means that the retention time measurements were carried out with samples containing only one particle size (8or15μm). Additionally, experiments with a particle mix were carried out in order to show a real separation between particles types. Movies at the outlet were recorded for demonstration. Figure 6.1 shows an example of separated particles (8μm and 15μm). The smaller particles which have a higher mean velocity are leading and afterward the larger ones arrive.

Unfortunately the sample containing the particles is already spread when injected into the separation channel. This means that the particles do not arrive in well defined clusters, but with a certain distribution (see fig. 6.1).

Three major facts are responsible for that:

- In order to be able to trap the smaller particles the inlet region was broadened (fig. 6.2). A sample plug is after release being compressed in the same percentage as the channel width reduces. Volume conservation demands then for an elongation of the sample plug (fig. 6.2).

- The second and more important impact is that when more than one particle is being trapped (which has to be the case when a separation is desired) clustering can appear

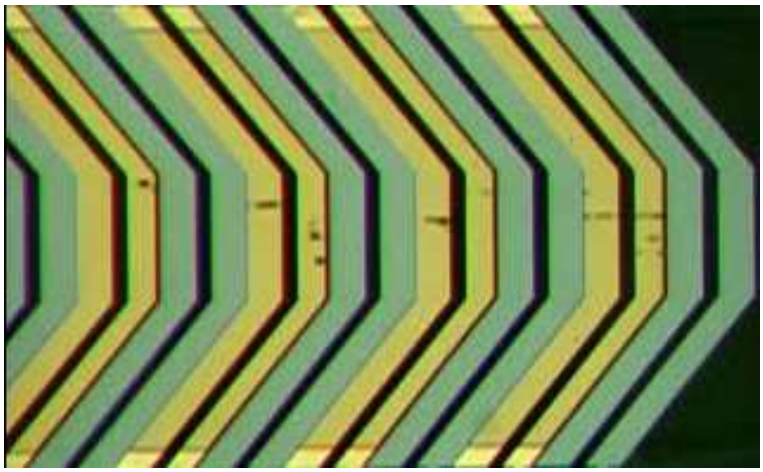

Figure 6.1: Image of separated particles (8 and 15μm) at the end of the channel (flow from left to right hand side). The smaller particles are faster (right) and the larger ones are slower (left).

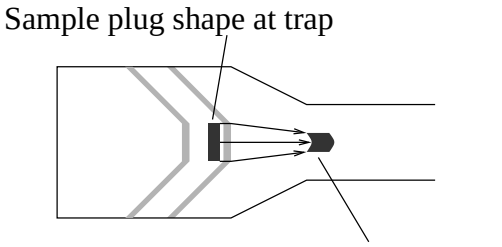

Figure 6.2: Sample plug elongation due to the tapered shape of the channel in the inlet region. The sample plug is compressed and therefore elongates in the same percentage as the channel width reduces.

(fig. 6.3). It was observed that these clusters tend to rotate due to the vertical velocity gradient. When the trap is deactivated these clusters break up but the actual vertical displacement of a single particle is not predictable. So different particles are released at different vertical displacements and are therefore exposed to different liquid velocities due to the parabolic flow profile. The error in time integrates until each particle reaches the separation channel (inside the channel they are forced on trajectories defined by the electric field gradient).

- Small differences in mass densities between liquid and particles also cause an error which is different for small and large particles. In the region between trap and separation channel where no guiding electric field gradient is present an additional gravity/buoyancy force cause the particles to sink (fig. 6.3). The vertical force equilibrium reads:

$$F_I = F_B - F_D \tag{6.1}$$

$$m\frac{dv}{dt} = g\frac{4}{3}r^3\pi\Delta\rho - 6\pi\eta r v_p \tag{6.2}$$

This differential equation has the time constant $\tau = \frac{m}{6\pi\eta r} = 13.1\mu s$ for a 15μm particle

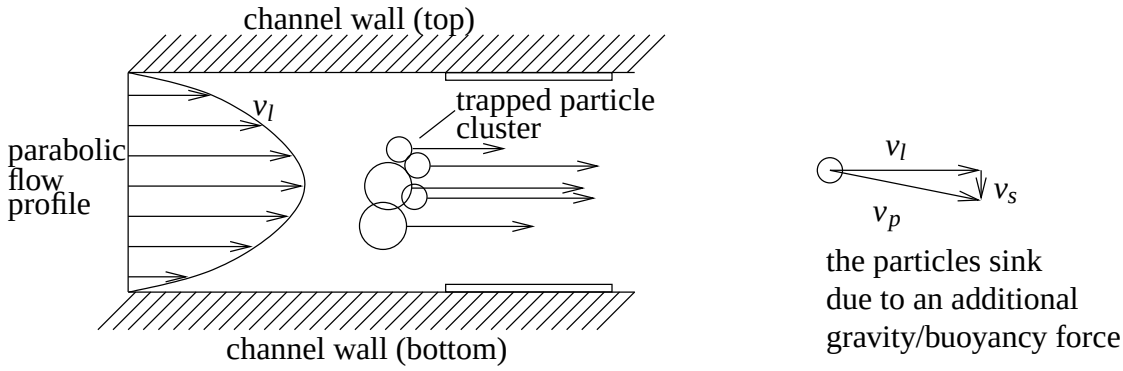

Figure 6.3: Different vertical displacements for single particles due to clustering. At the moment of release each particle is exposed to a different liquid velocity depending on its vertical displacement. After release the particles sink due to a buoyancy/gravity force.

which is small compared to the typical range of one second a particle needs to cover the distance between trap and separation channel. So the particles reach their settling velocity v_s almost immediately ($\frac{d}{dt} = 0$ in eq. (6.2)):

$$v_s = \frac{2r^2 g \Delta\rho}{3\eta} = \begin{cases} 18.36 \frac{\mu m}{s} \text{ for } 15\mu m \text{ particles} \\ \\ 0.522 \frac{\mu m}{s} \text{ for } 8\mu m \text{ particles} \end{cases} \tag{6.3}$$

v_s is the velocity a particle adopts in vertical direction when its not exposed to an electric field gradient.

This can be significant in the case of small flow rates. At a peak velocity of $1.6 \frac{mm}{s}$ a $15\mu m$ particle sinks approximately $13\mu m$ between trap and separation channel. For a $8\mu m$ particle its only $0.37\mu m$.

In section 6.2 proposals are given to overcome these problems.

6.2 Improvement for sample injection

For feasible separation results it is of importance that all particles belonging to a sample are injected at the same time. As mentioned above (sec. 6.1) the current trap structure does not bring good results. The sample is spread at the inlet and therefore the separation is not very reliable. This section discusses some proposals to overcome these issues.

The three items discussed in 6.1 which are responsible for a bad injection quality can be traced to the following properties:

- The *narrow* shaped part of the channel causes an elongation of the injected sample.
- Particles are released at different vertical displacements due to *lack of focusing forces* in the trap structure.

- A possible buoyancy/gravity force can cause an additional vertical displacement in the *long distance between trap and separation channel* which is not equipped with focusing elements.

These disadvantages are considered in the proposal for an improved trap structure (fig. 6.4). Here the narrow part is replaced by a straight channel. Please note that this demands for a

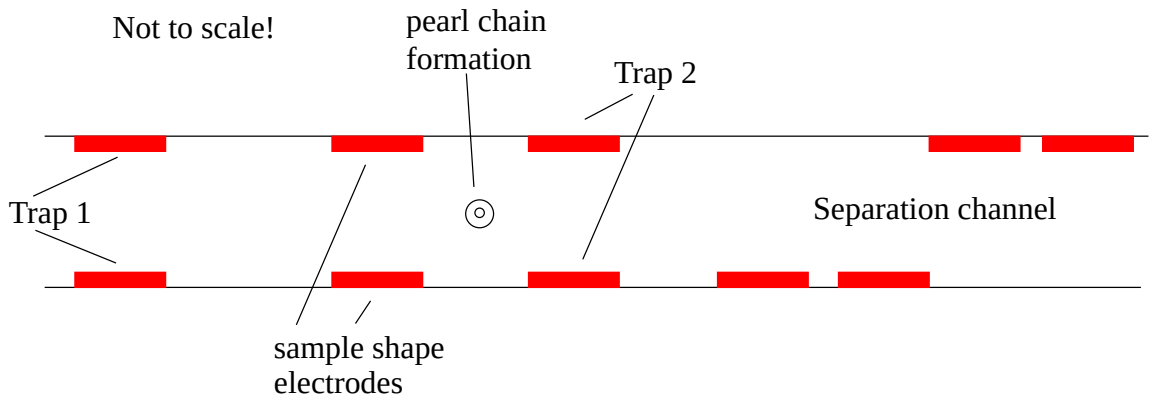

Figure 6.4: Improved trap structure for injection. Trap 1 as usual. Trap 2 has additional electrodes for shaping the sample to a pearl chain. So all particles are released at the same vertical displacement. If the narrow shaped part of the channel is omitted (no broadened channel at trap region) the separation channel can be placed immediately beneath the trap minimizing the impact of buoyancy/gravity forces. Furthermore the elongation of the sample due to the narrow channel part is eliminated.

decreased flow rate, such that the smaller particles can still be trapped. In this case no space has to be wasted for the narrow part and therefore the separation channel and the trap can be placed immediately behind each other. So the influence of the narrow shape (producing an elongated sample) and the impact of buoyancy/gravity forces on the particles (causing vertical displacements along the distance) are minimized.

Additional electrodes are used in the second trap to shape the particle sample to a pearl chain avoiding big clusters having the disadvantage of different vertical displacements at the moment of release.

6.3 Proposals for detection and sorting

In this project the detection or sorting of separated particles was not included. The most important task was to develop a separation system. However, there are ideas how to detect the separation process. In principle the detection system has to measure the retention time of different particles which is of importance in the case that the device is used as a sensor for measuring the particle size. Different possibilities can be considered:

- A laser could be used to mark particles of different fluorescent color depending on their size. Capturing images in a fixed time raster would allow an image processing program to distinguish particles by their fluorescent color. An additional filter for the excitation source would be required for the microscope and camera.

- It would also be possible to use an image processor to distinguish particles by their size (diameter). With a pattern recognition software images taken at different time steps could be used to trace the particles. In principle it would be possible to measure the particle size directly with this optical system but the time measurement together with a separation is much more sensitive (see fig. 5.6).

The latter possibility requires for a camera capable to trigger at defined time steps. High resolution in both cases is necessary in order to be able to recognize at least the $8\mu m$ particles.

In most cases the movie mode of digital still cameras has a too small resolution for this task. Additionally it is not necessary to acquire 25 images per second. Less images but with higher resolution cause the same amount of data but includes more information.

In order to get a spatial separation a dielectrophoretic sorter [NV03] could be added at the end of the separation channel. With an appropriate control system which operates the trap and the sorter electrodes it should be possible to define radius boundaries between which the particles are sorted. This offers the usage of this device as a particle size sensor (by defining a *radius window*) as well as the application as an accumulator for a specific particle species.

6.4 Outlook

There are several ideas how this project could be continued:

- The existing model uses a first order approximation for the dielectrophoretic force. Some further developments could be conducted to increase the accuracy by using a multi-order model (see [JW96] and [WJ96]).
- For more precise measurements an automatic detection system would be necessary. Integrating this into the existing design would allow for a better comparison between measurements and model.
- Exploiting the high sensitivity on radius variations the device could be adapted to measure size distributions of particle samples. An integrated optical detection system could be utilized for counting the particles in a time grid. A histogram of the particle distribution would be the result.
- Another direction of research could be the search for concrete application and the adaption of the device to such scenarios. For example the direct connection of the electrodes and the liquid could turn out as a problem for an application due to the liquid conductivity. The impact of an additional insulation layer on the field distribution should therefore be investigated. For a biological application it would also be necessary to determine the maximum electric field a biological object may be exposed to.

Conclusions

A particle separator chip based on dielectrophoresis was developed in this project. The device is capable of establishing a separation between particles of different size (8 and 15μm were used in the experiments). The separation channel was simulated, designed and manufactured. Retention time measurements with different particles for characterizing the device yielded the proof of principle.

A real separation of a particle mix was also demonstrated and recorded using a video camera.

The designed injection does not function very well. However, design adaptions will very likely improve the injection performance.

The project results have been described in an abstract submitted to the μTAS coference. The work has been accepted as an oral presentation at this conference which will take place in September 2004 in Malmö Sweden (see appendix D).

Appendix A

Model implementation in Matlab

A.1 model.m

```
parse='noo';
parse='yes';
if (parse=='yes')
    clear;
    filename='data/devicemainmain_el_field.dat';
    displacementstep_x = 2e-6;
    displacementstep_y = 2e-6;
    %particle description:
    r =4e-6;          % unit meters! 4 to 7.5*10-6m
    rho = 1.05e3;       %in kg/m^3
    etha = 1.002e-3;    %unit Ns/m^2
    k1 = 6*pi*etha*r;   %radius dependent
    m = 4/3*pi*rho*r*r*r;    %mass
    %get field data
    v_fluid_orig=dlmread('data/velocity_1D.dat', ';'); %returns x-component of velocity
    [FX,FY] = parse(filename, r, displacementstep_x, displacementstep_y);
end;

%prepare big matrices for long device calculation
if(strcmp(filename, 'data/devicemainmain_el_field.dat'))
    first=190;     %cut at this node (exact center)
    last=290;       %this is the coordinate/2 in the designer!
end;

FX_1=(cut_columns(FX, 1,first+1))';
FX_2=(cut_columns(FX, first+2, last+1))';
FX_3=fliplr((cut_columns(FX, first+1, last))');
FY_1=(cut_columns(FY, 1,first+1))';
FY_2=(cut_columns(FY, first+2, last+1))';
FY_3=fliplr((cut_columns(FY, first+1, last))');
FX=FX_1;
FY=FY_1;
for i=1:21
    FX=[FX FX_2 FX_3];
    FY=[FY FY_2 FY_3];
end;
FX=FX';
FY=FY';
%parameters:

forcefactor=0.145;
velocityfactor = 0.83;

v_fluid=v_fluid_orig*velocityfactor;
%maximum displacement
s=size(FX);
y_index_max=s(2)-1;
y_index_min=1;
x_index_max=s(1);
%time resolution and endtime
endtime = 15;
timestep = 0.001;

%start point coordinates and initial conditions
x0 = 200e-6;
y0 = 35e-6;
v0_x = 0;
v0_y = 0;

%initial values of loop variables
x=x0;
y=y0;
```

```
i=1;

for t=0:timestep:endtime
    %calculate weighted mean values of forces
    x_index = double(int32(x/displacementstep_x))+1;
    if x_index >= x_index_max
        break;
    end;
    y_index = double(int32(y/displacementstep_y))+1;
    if y_index > y_index_max
        y_index = y_index_max;
    end;
    if y_index < y_index_min
        y_index = y_index_min;
    end;

    weight_x = (x-(x_index-1)*displacementstep_x)/displacementstep_x;  %[0..1]
    weight_y = (y-(y_index-1)*displacementstep_y)/displacementstep_y;
    x_i=x_index;
    y_i=y_index;
    Ff_x=(FX(int32(x_i),int32(y_i))*(1-weight_x)+FX(int32(x_i+1),int32(y_i))*(weight_x))*(1-weight_y) +
        (FX(int32(x_i),int32(y_i+1))*(1-weight_x)+FX(int32(x_i+1),int32(y_i+1))*(weight_x))*weight_y;
    Ff_y=(FY(int32(x_i),int32(y_i))*(1-weight_x)+FY(int32(x_i+1),int32(y_i))*(weight_x))*(1-weight_y) +
        (FY(int32(x_i),int32(y_i+1))*(1-weight_x)+FY(int32(x_i+1),int32(y_i+1))*(weight_x))*weight_y;
    Ff_x=Ff_x*forcefactor;
    Ff_y=Ff_y*forcefactor;
    velocity_x = v_fluid(int32(y_index+1))*weight_y + v_fluid(int32(y_index))*(1-weight_y);

    %displacement for one timestep
    delta_x = quadl(@velocity, 0, timestep, [], [], v_fluid(int32(y_index)), v0_x, Ff_x, k1, m);
    delta_y = quadl(@velocity, 0, timestep, [], [], 0, v0_y, Ff_y, k1, m);
    v0_x = velocity(timestep, v_fluid(int32(y_index)), v0_x, Ff_x, k1, m);
    v0_y = velocity(timestep, 0, v0_y, Ff_y, k1, m);
    x=x+delta_x;
    y=y+delta_y;
    x_vector (i)=x;
    y_vector (i)=y;

    %necessary for additional plots
    forcereminder(i)=Ff_x;
    drag_force(i)=6*pi*etha*r*(velocity_x-v0_x);

    i=i+1;

end;
 figure;
 plot(x_vector, y_vector);
 axis([0 max(x_vector) 0 7e-5]);
 xlabel('displacement in x-direction (m)');
 ylabel('displacement in height (m)');
 legend('particle path');
 v=gradient(x_vector, timestep);
 a=gradient(v, timestep);
 f_inertia = m*a;
 s=size(x_vector);
 figure;
 subplot(4,1,1);plot(x_vector,v);legend('particle velocity')
 subplot(4,1,2);plot(x_vector,f_inertia);legend('inertia force');
 subplot(4,1,3);plot(x_vector,forcereminder);legend('DEP force on particle');
 subplot(4,1,4);plot(x_vector,drag_force);legend('drag force on particle');
 xlabel('displacement x [mu m]');
```

A.2 parse.m

```
function  [FX,FY] = parse(filename_elfield, r, displacementstep_x, displacementstep_y)
%parses a file exported in coventorware and returns a matrix containing
%the dielectrophoresis force in each point of the mesh
M=dlmread(filename_elfield, ';');
s=size(M);
y_min=min(M(:,2));
y_max=max(M(:,2));
matrixsize=s(1);

%make a matrix with index 1,2,3,...
for i=1:matrixsize      %loop through whole matrix of file
    if ((M(i,2)~=y_min)&(M(i,2)~=y_max))    %cut electrode space
        %calculate abs value of el. field
        abs_E=(10^6*sqrt(M(i,9)^2+M(i,10)^2+M(i,11)^2))^2; %(V/m)^2
        %calculate integer coordinates corresponding to matrix indices
        x=round((M(i,1)*1e-6)/displacementstep_x+1);
        y=round((M(i,2)*1e-6-0.25e-6)/displacementstep_y+1);
        z=round(M(i,3)/1000+1);
        elField(x,y,z) = abs_E;
    end;
end;

s=size(elField);
```

```
%pick out one slice
slice_z=1;
for x=1:s(1)
    for y=1:s(2)
        sl(x,y)=elField(x,y,slice_z);
    end;
end;

%calculate gradient
[FY,FX]=gradient(sl,displacementstep_x,displacementstep_y);

%calculate force

K=-0.48;              % estemated clausius mosotti value
eps0 = 8.8542e-12;
eps_medium = 80;
for x=1:s(1)
    for y=1:s(2)
        FX(x, y)=2*pi*eps_medium*eps0*r^3*K*FX(x, y);
        FY(x, y)=2*pi*eps_medium*eps0*r^3*K*FY(x, y);
    end;
end;
```

Appendix B

Metalization and electrode patterning

Since the bottom wafer of the device is equipped with through holes its process for electrode patterning is more complicated than for the top wafer. While the resist for the top wafer can be processed with a common spin method, the bottom wafer must be treated with a spray coater. Holes in the wafer would cause unevennesses in the resist layer. Therefore two different processes had to be applied.

First the glass wafers were cleaned with a Megasonic Cleaner. This cleaner has a nozzle where a jet containing a NH_3OH solution can be generated. Furthermore this nozzle transmits a surface wave via the jet to the spinning wafer (1500 RPM). So larger contamination is removed by vibrations and organic adhesions are cracked by the NH_3OH solution.

The process of the **top wafer** continues with the metal deposition. At a pressure of $10^{-7} mbar$ first a $50nm$ Cr layer and then the $200nm$ Au layer was deposited. Cr is necessary as a compound layer between glass and Au.

For the lithography a positive resist (Clariant AZ 15 12 HS) was spun on and dried on a hot plate at $90°C$ for 5 minutes. Then the wafer was exposed using the top electrode mask. After that the metal layer was etched with the following chemicals:

- Solution used for etching Au:
  - 25g J
  - 50g KJ
  - 250ml H_2O
- Solution used for etching Cr:
  - 85g $Ce(NH_4)_2(NO_3)_6$
  - 45ml HNO_3
  - 450ml H_2O

For the **bottom wafer** a lift off technology was used for patterning the electrodes. Since this wafer is equipped with through holes it is not possible to use the conventional spinning technique. So a spray coater had to be used for depositing the resist.

After the exposure with an inverted mask (fig. B.1a) the exposed areas (fig. B.1b) are cross-linked in a bake step (fig. B.1c). A flood exposure of the whole wafer makes the areas which

were not exposed first soluble for the developer (fig. B.1c). After developing, the resist which was exposed first remains with an undercut (fig. B.1d). After a metalization step (fig. B.1e), which is the same as used for the top wafer, the remaining resist covered with metal can be stripped off (fig. B.1f). This technology is called *image reversal technology* and is described in detail in [Mic04].

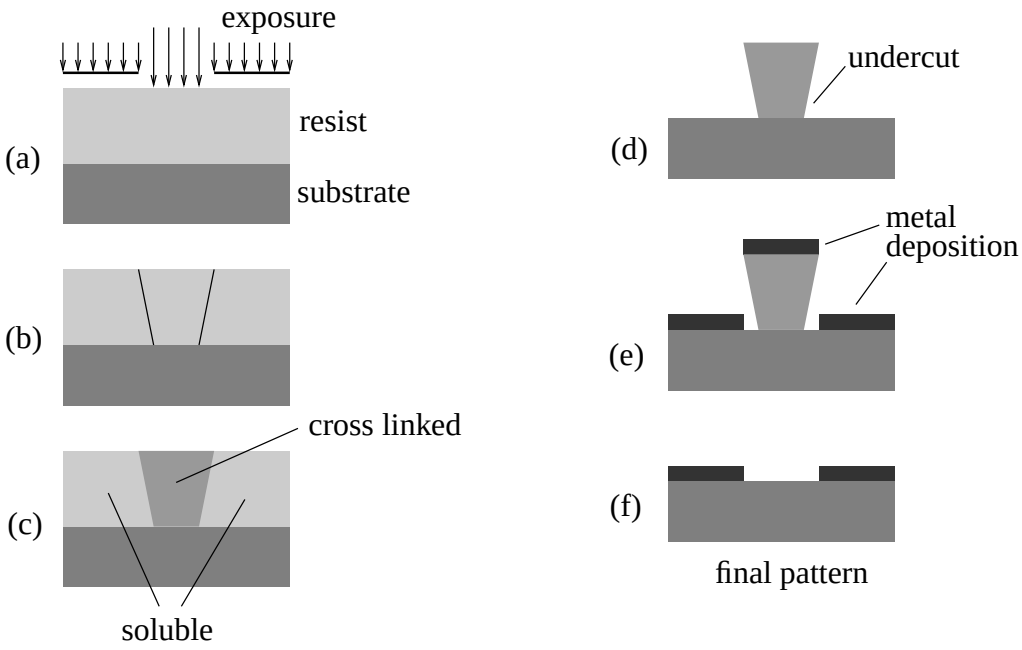

Figure B.1: Process flow of lift off electrode patterning. (a)

Appendix C

Trap characterization

Since the development of a separation channel was the main goal in this project the trap structure can be seen as a necessary but not crucial part of the scientific work. A measurement of the release point of a dielectrophoretic trap would demand for another setup than used in our case.

However, it was observed that much higher voltages are necessary to trap the particles in the liquid drag. So we decided to try to find the point of release by activating the traps and reducing the voltage until particles were released.

It is of importance to mention that this determination of the point of release is a more practical approach and cannot directly be compared to the model which deals only with single particle. In the real trap there are particle clusters which behave different. An accurate determination and comparison between experiment and simulation for DEP traps (including higher order moments) is given in [VBT$^+$01].

Table C.1 shows typical trap voltages for different flow rates at which trapping was observed. These values were not confirmed by a large number of measurements.

Compared to the simulation for single particles much higher voltages are necessary for trapping. The reason for that behavior can be found in the neglect of higher order moments in the simulation. Additionally mechanical vibrations and clustering is not taken into account.

flow rate in $[\mu l/min]$	U_{trap} in $[V]$
0.84	4.1
1.68	6.7
2.52	10.2
3.36	12
4.2	xx

Table C.1: Typical voltages at which trapping was observed for different flow rates with $8\mu m$ particles. At a flow rate of $4.2\mu l/min$ it was not possible to trap these particles. Note that the values are practical quantities which were not confirmed by a number of measurements.

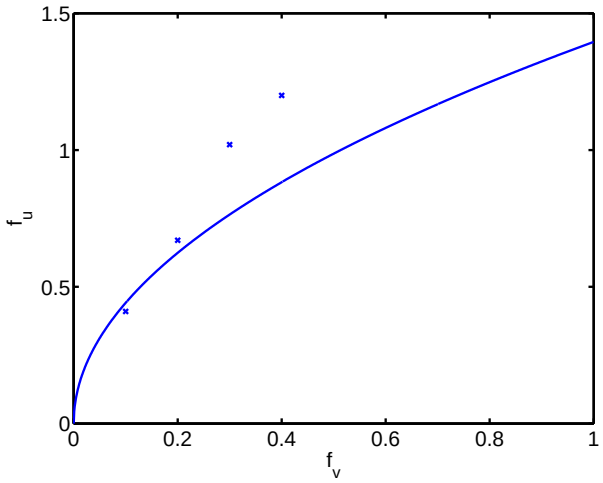

Figure C.1: Comparison of predicted trapping conditions and observed values. Clustering, mechanical vibrations and higher order moments are neglected in the model. Much higher voltages are necessary to trap the particles. This qualitative behavior matches with the effects observed in [VBT$^+$01]. With higher voltages the resulting DEP force decreases due to gaining higher order terms.

Appendix D

Abstract for μTAS conference

Topic No. 5.4
Oral Presentation preferred

Continuous Particle Separator based on periodical DEP Elements

S. Kostner[1], J.H. Nieuwenhuis[1], P. Svasek[2], A. Jachimowicz[1], M.J. Vellekoop[1]

[1]Institute for Sensor and Actuator systems (ISAS), Vienna University of Technology, Gusshausstrasse 27-29, A-1040 Vienna, Austria, email kostner@isas.tuwien.ac.at
[2]Ludwig Boltzmann Institute of Biomedical Microtechnology, Vienna, Austria

Keywords: dielectrophoresis, particles, separator

Introduction

In this work a novel device for continuous separation of particles based on dielectrophoresis (DEP) is presented (Fig. 1). As the particles flow through the separation channel, dielectrophoretic forces are applied to move them up and down, which results in a sinusoidal trajectory (Fig. 2). The amplitude of this sinusoid strongly depends on the particle size. Since the velocity profile of the liquid in a pressure driven flow is parabolic, the flow-speed of a particle depends on its vertical position in the channel. Larger particles (for which the amplitude of the sinusoidal trajectory is larger) will now have a lower average velocity, which results in longer retention time than smaller particles. At the end of the channel there will be a separation of particles depending on their diameter. This device does not use gravity as a parameter for separation, as in other devices [e.g. 1].

Device

The device consists of two glass slices bonded together with SU-8 [2], which also defines the channel dimensions. The liquid connections are defined by through holes in one of the glass wafers. The DEP electrodes (Cr/Au) are 80µm wide.
The separation channel has a periodic electrode structure to generate strong non-uniform electric fields. Because the electrodes are applied on both top and bottom the particles move around the middle of the channel, minimizing the influence of gravity. A simple particle trap structure was used to accumulate and periodically release the particles, allowing for continuous operation of the device. So, both sample injection and separation are controlled electronically.
A dynamic simulation model has been developed to optimize the electrode structure and to estimate the voltage necessary for trapping the particles. The force equilibrium between dielectrophoretic-, drag- and inertial forces is calculated from which the particle trajectory is determined (fig. 3). The difference in retention time is a measure for the separation efficiency.

Experimental results

Polystyrene particles of 8 and 15 µm diameter suspended in deionized water were pumped through the device using a syringe pump and the retention time of the particles was measured. At a DEP voltage of 5.5 V (RMS, 1 MHz) the larger particles show an average 19% longer retention time than the smaller particles, which proofs the concept (Table 1). A histogram for several measurement series is shown in Fig. 4.

Conclusion

We have simulated, designed and fabricated a novel particle separation device based on periodic DEP elements. Our first measurements demonstrate, that particles of 8 and 15µm show significant differences in retention time (19%) at a DEP voltage of 5.5 V (RMS, 1 MHz).

References:

[1] H. Sano, H. Kabata, O. Kurosawa, M. Washizu, "Dielectrophoretic chromatography with cross-flow injection", The Fifteenth IEEE International Conference on Micro Electro Mechanical Systems, 2002, 20-24 Jan. 2002, pp. 11-14

[2] P. Svasek, E. Svasek, B. Lendl, M.J. Vellekoop, "SU-8-Based Fluidic Devices", proc. of Eurosensors XVII, September 21-24, 2003, Guimaraes, Portugal, 2003, pp. 283-286

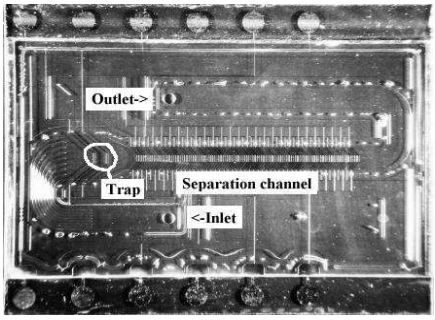

Figure 1 Particle separation chip (1.5x2 cm^2). Channel height 70µm, width 1mm, length 10.4mm. The separation channel has 26 DEP elements.

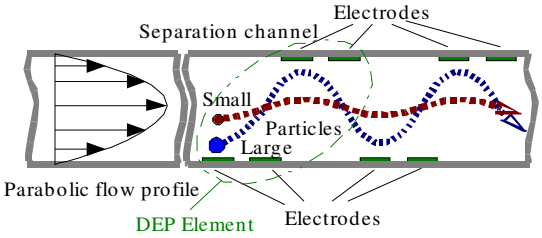

Figure 2 Schematic representation of the cross section of the flow channel (showing two DEP elements with four electrodes each). Particles follow a sinusoidal trajectory caused by dielectrophoretic forces, generated by the electrodes in the channel.

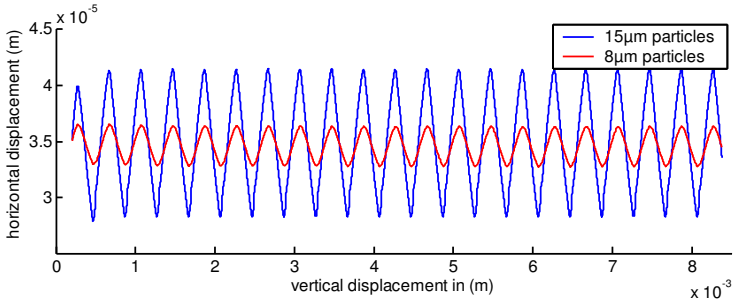

Figure 3 Simulation of the particle trajectories in the separation channel for 8 and 15µm diameter particles.

Particle Size	Mean retention time
8µm	8s
15µm	9.5s

Table 1 Measured mean retention time for different particle sizes.

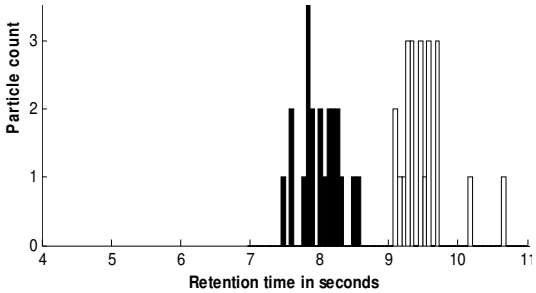

Figure 4 Histogram for measurements of retention time with different particle sizes; 8µm (black) and 15µm (white); 22 measurements per size.

Bibliography

[BE02] Robert W. Barber and David R. Emerson. Numerical simulation of low reynolds number slip flow past a confined microsphere. *23rd International Symposium on Rarefied Gas Dynamics*, 2002.

[Jon95] Thomas B. Jones. *Electromechanics of Particles*. Press Syndicate of the University of Cambridge, 1995.

[JW96] Thomas B. Jones and Masao Washizu. Multipolar dielectrophoresis and electrorotation theory. *Journal of Electrostatics*, 37:121–134, 1996.

[Mic04] MicroChemicals GmbH, Schillerstrasse 18, D-89077 Ulm. *TI 35ES Technical Data Sheet*, 2004.

[NV03] Jeroen H. Nieuwenhuis and Michiel J. Vellekoop. Improved dielectrophoretic particle actuators for microfluidics. *Proceedings of IEEE Sensors*, 1, 2003.

[SKKW02] Hikari Sano, Hiroyuki Kabata, Osamu Kurosawa, and Masao Washizu. Dielectrophoretic chromatography with cross-flow injection. *The Fifteenth IEEE International Conference on Micro Electro Mechanical Systems*, 2002.

[SSLV03] Peter Svasek, Edeltraut Svasek, Bernhard Lendl, and Michiel Vellekoop. Su-8-based fluidic devices. *17th European Conference on Solid-State Transducers (Eurosensors XVII)*, 2003.

[VBT+01] Joel Voldman, Rebecca A. Braff, Mehmet Toner, Martha L. Gray, and Martin Schmidt. Holding forces of single-particle dielectrophoretic traps. *Biophysical Journal*, 80:531–541, 2001.

[Whi01] Frank M. White. *Fluid Mechanics*. McGraw-Hill Higher Education, fourth edition, 2001.

[WJ96] Masao Washizu and Thomas B. Jones. Generalized multipolar dielectrophoretic force and electrorotational torque calculation. *Journal of Electrostatics*, 38:199–211, 1996.